Tough Polyampholyte Hydrogels: Effect of Dialysis and Their Applications in Stretchable Electronic Skins

by

Hemant Charaya

A thesis submitted in partial fulfillment of the requirements for the degree of

Master of Science

in

MATERIALS ENGINEERING

Department of Chemical and Materials Engineering
University of Alberta

Abstract

Tough hydrogels are an emerging class of advanced materials that have resolved the long-standing problem of brittleness and fragility in conventional hydrogels. Their superior mechanical performances enable several unprecedented applications in bio-integrated electronics, surgical glues, and soft sensors and actuators. Polyampholyte (PAm) hydrogels are a sub-class of tough hydrogels which are formed by inter/intra chain ionic complexes between counter charged functional groups present on the polymer chains. The unique chemistry and structure of PAm hydrogels make them highly tough, resistant to biofouling, self-healing and adhesive on various surfaces. In this thesis, we have explored the potential of these tough PAm hydrogels as a key material for energy storage devices and for wearable electronics.

Overall, this thesis has been divided into two sections. In the first section, we have emboldened the idea of using tough PAm hydrogels as gel electrolyte for energy applications by showing their ability to maintain good mechanical properties while delivering high ionic conductivity. Here, we studied the behavior of PAm hydrogels dialyzed in common electrolyte solutions while carrying out a systematic investigation of how specific ions influence the ionic complexes of tough PAm hydrogels. In the second section, we have utilized the PAm hydrogels as self-adhesive, transparent and stretchable electrodes to build a thermochromic liquid crystal-based skin-like wearable electronic device that can carry out dual detection of tactile and temperature sensation simultaneously. This device provides a facile and an inexpensive platform for smart electronic skins for biomedical and internet of things applications.

Preface

(Mandatory due to collaborative work)

This thesis is organized in five chapters.

Chapter 1 is the introduction

Chapter 2 of this thesis has been published as: H.-J. Chung, H. Charaya, L. Liu, X. Li, "Tough Hydrogels: Toughening mechanism and their utilization of in Stretchable Electronics and Regenerative Medicines", Hybrid Organic and Inorganic Interfaces: Towards Advanced Functional Materials, **2018**: 535-580. Only the toughening mechanism section of this manuscript is borrowed in Chapter 1, which was written by H. Charaya and revised by H.-J. Chung.

Chapter 3 of this thesis has been prepared for submission as H. Charaya, X. Li, N. Jen, H.-J. Chung, "Effect of Dialysis on Conductivity and Mechanical Properties of Tough Polyampholyte Hydrogels". H. Charaya and H.-J. Chung conceived the idea. H. Charaya performed all the measurements with the help of X. Li & N. Jen. Data interpretation was carried out under the guidance of X. Li and H.-J. Chung. H. Charaya wrote the manuscript which was revised by X. Li and H.-J. Chung.

Chapter 4 of this thesis has been prepared for submission as: H. Charaya, T.-G. La, S. Qiu, X. Li, H.-J. Chung, "Stretchable Electronic Skin with Colorimetric Temperature Sensing and Capacitive Pressure Sensing Abilities". H. Charaya, T.-G. La, and H.-J. Chung conceived the idea. H. Charaya, T.-G. La and S. Qiu performed the experiments. H. Charaya carried out data interpretation under the guidance of T.-G La, X. Li and H.-J. Chung. H. Charaya wrote the manuscript which was revised by T.-G. La and H.-J. Chung.

Chapter 5 includes a summary of overall conclusions of this thesis

Acknowledgement

First and foremost, I would like to express my sincere gratitude to my mentor and supervisor Dr. Hyun-Joong Chung for his continuous support and encouragement during the course of my degree. For more than two years, he has constantly inspired me with his own enthusiasm and dedication for research. I deeply appreciate all his contributions to make my MSc experience, at the University of Alberta, a joyful and pleasant one. I would also like to thank him for his immense patience and continuous care to let me, like many of his other students, evolve into a better research scholar.

I am extremely thankful to all the past and present members of my research group with whom I had the pleasure to work with or alongside. Particularly, I want to acknowledge Xinda Li, a PhD scholar from our group, who was ever-present to help me with his expertise in hydrogels and stretchable electronics during this time. Outside my research group, I was fortunate to have a mentor in Kaushik Sivaramakrishnan who was always there to guide me to the right path.

Finally, I wish to express my love and gratitude to my parents and siblings who are the pillars of my strength and have provided me with unconditional support throughout my life.

Hemant Charaya

April 2018

Table of Contents

List of Tables

List of Figures

Chapter 1. Introduction

1.1 Background

Hydrogel can be defined as a network of physically or chemically crosslinked polymer chains which swell in water. For a typical hydrogel, water constitutes 70-80 % of their total weight which is similar to the composition of human tissues and cartilages. Owing to their ability to accommodate large amount of water inside polymer matrix, hydrogels perform central role in many of our everyday-use products such as baby diapers, contact lenses and moisturizing patches. The equilibrium swelling of a hydrogel is essentially governed by the competition between the swelling and elastic forces: The swelling forces comes from polymer-water interaction, electrostatic interaction between polymer chains and osmotic pressure due to counter-ion concentration difference between inside and outside of the gel, while the elastic forces generates from the crosslinking of the polymer network (1). By selecting suitable monomer units and crosslinking type, we can synthesize hydrogels that can respond to specific external stimuli, like temperature, electric field, pH or salt concentration of the solvent. This makes hydrogels smart functional materials with potential in wide range of applications such as bio-sensors, actuators, drug delivery etc. For example, thermo-responsive polyvinyl-isopropyl acrylamide (PNIPAAm) hydrogels have been widely studied for controlled drug delivery application as they undergo reversible phase transition, from swollen hydrated state to dehydrated state, at 32^{o}C which is close to human body temperature (2). Similarly, weak polyelectrolyte hydrogels are also a suitable material for drug delivery and bio-molecule sensing (3) as they encounter abrupt volume change when pH of the solvent crosses pKa value of ionic functional groups present on the polymer chains. Once polymer chains attain fixed charges, polyelectrolyte hydrogels can also be actuated by

applying electric field across them for potential usage as electroactive actuators (4). In addition to the usage as stimuli-responsive materials, hydrogels are also an excellent material for tissue engineering as their high-water content makes them compatible with living tissues. Further, their porous structure provides efficient supply of nutrients and removal of metabolites which renders them an ideal candidate for preparing scaffolds in tissue engineering (5).

1.2 Progression from Conventional to Tough Hydrogels

As discussed above, synthetic hydrogel materials have attracted widespread attention due to their unique structure and properties. However, most of the synthetic hydrogels are mechanically weak, fragile and brittle which puts a constraint on the scope of their applications and restrict it to the domains like drug delivery and bio-sensing where mechanical strength of the hydrogels is of least importance. For broadening the horizon of hydrogel applications, this issue was first addressed at the start of 21st century when hydrogels, with homogeneous network structure, were synthesized by introducing slide ring crosslinkers (Slide-Ring hydrogels) (6) and employing four-armed PEG pre-polymers (tetra PEG hydrogels) (7) for hydrogel synthesis. Although, these hydrogels possessed good mechanical strength and showed high stretchability, but their mechanical properties were largely affected by the presence of a notches inside the material (8) (9). To curtail this effect of notches on mechanical properties of hydrogels, Dr. Gong at Hokkaido University proposed the idea of introducing sacrificial bonds to hydrogel network which breaks during deformation and absorb a lot of energy (10). Thus, these sacrificial bonds increase the fracture toughness of the hydrogels and prevent material failure by prohibiting the crack propagation. Based on this concept, over the past decade, there has been a surge of studies which have focused on improving the fracture toughness of the hydrogels and make them mechanically tough and highly stretchable. In recent times, with much improved mechanical properties, these

"tough hydrogels" have started to find applications in various unprecedented fields which were not, previously, associated with the field of hydrogels such as electroluminescent displays (11), stretchable smart windows (12), surgical glues, reliable and durable soft actuators (13), optical fibers (14) etc. With great numbers of new ideas and perspectives pouring along at rapid pace, in near future there will be more of such developments in practical applications of tough hydrogels, performing roles that were unforeseen before.

1.3 Tough Hydrogels in Stretchable Electronics & Energy Storage Devices

1.3.1 Stretchable Electronics

Since tough hydrogels have similar physiological and mechanical properties as human tissues, they have been regarded as an ideal substrate or matrix material to realize bio-integrated electronics devices. There are two key factors for using hydrogel as the substrate for stretchable electronics. First, the hydrogel must be mechanically tough and robust under large deformation. Second, the adhesion between the hydrogel and the target material must be strong. There have been several inspiring attempts to apply hydrogel as the substrate for stretchable electronics. Zhao *et al*. (15) used DN hydrogel as the functional substrate for various stretchable electronics and devices. They successfully integrated stretchable conductors, rigid electronic components, and drug delivery channels and reservoirs in the DN hydrogel matrices. Hydrogel with prescribed pattern was fabricated, where the pattern may serve in drug delivery. Electronic components (conductors, chips, transducers, resistors, capacitors) were encapsulated by polydimethylsiloxane to maintain their functionality in wet environment. Then, these components are attached to hydrogel surface by covalent bonding. In addition to stretchability, tough hydrogels also exhibit other novel functionalities. For example, high water content allows the hydrogels to contain water-soluble drugs, opening a possibility of controlled drug release. Another simple example is to put electronic

components in hydrogel precursor solution, followed by polymerization (16). In this case, interfacial bonding between the device and the hydrogel must somehow be achieved by harnessing the intrinsic chemical property of the synthesizing hydrogel.

The other elements of stretchable electronics where tough hydrogels have found immense attention, of late, is in the role of conductive materials which are stretchable, biocompatible and, most importantly, transparent. The presence of salt ions inside the hydrogel matrix render them ionically conductive. The fact that salt ion containing hydrogels are transparent, owing to their water content, has been well-exploited to construct stretchable electronic devices which requires transmission of electrical signals without obstructing the path of optical signals. So many impressive demonstrations such as transparent loudspeakers (17), touch panels (17) (18), e-skin (19), stretchable electroluminescent displays (11) (20), have been performed using this concept. In all these devices, ionic conductive hydrogels are used as electrode materials where a dielectric layer is sandwiched between two hydrogel layers. The hydrogel electrodes are connected to the power source using an electronic conductor which lie outside the active region of the device and thus, need not require to be transparent or stretchable. Replacing traditional electrode materials with hydrogels in this form requires overcoming the tendency to undergo electrochemical reactions at higher voltages. This is addressed by choosing suitable materials for electrical and ionic conductors such that they form a stable electric double layer (EDL) i.e. electrons and ions do not cross the interface to instigate electrolysis process (11). It has been assessed that as-long-as the voltage between electrode and ionic conductor lies in the range of $\pm$ 1V (19), the EDL layer remains stable and no electrochemical reaction takes place.

1.3.2 Energy Storage Devices

When swollen with aqueous electrolyte solutions, hydrogels can be used as electrolyte in energy storage applications (e.g., in battery and in supercapacitor), which is also called aqueous gel polymer electrolytes. The gel polymer electrolytes, classified as a category of solid-state electrolytes, possess combined merits of freestanding properties of solid systems and liquid-like transport properties. The merits include competitive ionic conductivity (comparable with pure liquids), absence of leakage problems (no need for high-duty packaging to prevent liquid leakage), and simpler device configuration for device fabrication (no need for separator) (21). Because organic solvents are often toxic and expensive, aqueous gel polymer (i.e., hydrogel electrolyte) is more desirable. Hydrogel electrolytes can be made to be stretchable, flexible, and healable, thus endowing some novel functionality to conventional electrochemical energy storage devices. Poly (vinyl alcohol) (PVA) doped with proton alkaline is one of the widely used aqueous gel polymer electrolytes (22) (23). PVA/LiCl hydrogel was also developed by Wang *et al*. for lithium ion battery application (24). An excellent gel is electrolyte is defined by its high ionic conductivity, for good electrochemical performance (25), and mechanical robustness, for maintaining device's structural integrity (26). For conventional hydrogels, any attempt to increase the ionic conductivity, by inserting salt ions into the polymer matrix, drastically impairs its mechanical properties. Thus, it is very difficult to reach a stage where high conductivity of the hydrogel is complemented with reasonable mechanical robustness. At this juncture, tough hydrogels promise to play a major role in overcoming this issue with gel polymer electrolytes in energy storage devices.

A slight paradigm shift has happened with the role of hydrogel materials in energy storage devices, in recent times, as conductive polymer hydrogels (CPHs) have found application as

electrode materials. Highly porous microstructures of CPHs provide a large electrochemical interface for electrolyte ions which leads to highly efficient ion/electron transport (27). This helps in improving the electrochemical performance of the device. For examples, Shi *et al*. fabricated a conductive polypyrrole (PPy) hydrogel electrodes which showed a very good specific capacitance value of 400 Fg^{-1} at discharging rate of 0.14Ag^{-1} (28). 3-D hydrogel network of polyaniline (PAni) have also been investigated for application in electrochemical supercapacitors. In addition to a specific capacitance values of 480 Fg^{-1} (discharging rate= 0.20 Ag^{-1}), they also showed excellent rate capability for performance at high power (only ~7 % capacitance loss upon increasing current density from 0.5 Ag^{-1} to 5 Ag^{-1}) (29). The other major reason for pursuing with CPHs as electrode material is their ability to accommodate large amount of strains during electrochemical reactions which contributes to very good cyclic stability of the device during charging and discharging cycles. Incorporating tough CPHs as electrodes, in future, will potentially further enhance this cyclic stability of the energy storage devices.

1.4 Scope & Outline of this Thesis

In a nutshell, this thesis is a stride to take a step forward in the direction of finding the engineering applications of tough hydrogels from an end-user perspective. In this work we have proposed the idea of using tough polyampholyte (PAm) hydrogels: (1) as mechanically robust and highly conductive gel electrolyte for energy storage devices and (2) as stretchable, transparent and ionically conductive electrodes for an electronic skin. So far, in literature, most of hydrogel applications are based on tough double network (DN) hydrogels. However, in this work, we have employed PAm hydrogels instead of DN hydrogels because of their single-step synthesis, which is important during scaling up the process, and their fatigue resistance i.e. they don't leave any residual strain upon deformation and release.

Chapter 2 of this thesis covers the fracture mechanics of hyper-elastic materials such as elastomers and hydrogels while explaining the reasons behind mechanical weakness of conventional synthetic hydrogels. This is followed up by a comprehensive discussion on the physics behind the toughening mechanism involve in different classes of tough hydrogels.

In Chapter 3 we have studied different ways in which foreign electrolyte ions interact with ionic complexes of tough PAm hydrogels upon their dialysis, and how this affects their ionic conductivity and mechanical properties. This study is intended to provide principle idea for designing gel electrolytes based on tough PAm hydrogels.

In Chapter 4 we have introduced a thermochromic liquid crystal (TLC) based bi-functional e-skin device for simultaneous tactile and temperature sensing. Here, we have used laser-cut PAm hydrogel patterns as ionically conductive electrodes for capacitive-pressure measurements while, simultaneously, exploiting their transparent nature for temperature measurement from color-temperature interplay of TLC material.

The overall conclusions of the thesis are summarized in Chapter 5.

Chapter 2. Toughening Mechanism in "Tough Hydrogels"

2.1 Introduction

Before proceeding to the results of our studies, we found that it is essential for a reader understand the physical origin of the toughening mechanism in "tough hydrogels". Therefore, in this chapter we have individually discussed how toughness enhancement is achieved in different classes of tough hydrogels. Here, at first, we will briefly survey the role of fracture energy in determining the material's *fracture toughness*, which is the key concept to define the merit of tough hydrogels. It is notable that the fracture toughness, which is associated with pre-existing cracks in the sample, is a different concept from tensile toughness that is typically determined from flawless samples. For hydrogels, easy crack propagation that leads to tear has been the biggest challenge (imagine Jell-O after tapping with the edge of spoon). After that we will define some key concepts associated with the fracture toughness of hyper-elastic materials such as elastomers and hydrogels. Finally, in Section 2.4 we will use these concepts to classify tough hydrogels on the basis of their toughening mechanism.

2.2 Fracture Energy

Inglis established an important foundation to understand material fracture in 1913 when he found out that the stress distribution changes quite dramatically near the elliptical hole in a linear elastic sheet (30). The stress at any point inside a material has an inverse relation with the square root of the distance from the crack (r), as shown in equation 2.1:

$$\sigma_r = \frac{\sigma_\infty}{\sqrt{r}} \qquad 2.1$$

where, σ_∞ is the applied stress. From equation 2.1, the value of stress approaches to ∞ at the crack tip ($r \to 0$). If the material is linearly elastic, that is, following Hooke's law, one would assume this stress to overcome the cohesive strength of the material, thus crack should grow continuously. In real material case, (i) there is a threshold criterion for a crack to propagate inside a material, which governs the toughness of the material, and (ii) a "process zone", where the threshold criterion fails, is formed near the crack tip (31). In the process zone, the linear elasticity of the material no longer holds due to complications such as plastic deformation, viscoelasticity, and other nonlinear elastic responses. Such effects dissipate energy from crack tip, thus toughening the fracture toughness of the material. It is fair to state that these nonlinear effects are not fully understood (31). Determining the size of the process zone is the key to understand the failure of a given material. When process zone is smaller in size when compared with the characteristic length scale, most of the energy release during crack propagation comes from the stored elastic energy (31). This case is popularly known as "small-scale yielding." In this case, one can effectively easily ignore the process zone and interpret the stress value outside of this region with high accuracy: $\sigma_r \cong K/\sqrt{r}$, where K is the stress intensity factor. Once the energy dissipation in the process zone is discounted, the only energy interaction for the crack propagation is between the release of stored elastic energy and the energy required to create two new surfaces. Griffith proposed a theory by accounting the energy interactions, later referred as Griffith theory, which sets the foundation of linear elastic fracture mechanics (LEFM) (32). The theory states that for linear elastic materials, the crack of length, c, grows by ∂c, only if the absolute value of decrease in strain energy ($\partial W/W$), stored inside a material, is more than the energy required to produce two new surfaces ($\Gamma \partial$A, Γ being the surface energy per unit area):

$$-\frac{\partial W}{\partial c} = \Gamma \frac{\partial A}{\partial c} \qquad 2.2$$

Inspired by Griffith energy criterion, Irwin calculated the value of energy flow, G, to the crack tip with per unit of crack extension that is given by (33)

$$G = \frac{1-\upsilon^2}{E}\, K_I^2 \qquad 2.3$$

where υ and E are Poisson's ratio and elastic modulus of the material, respectively; G is the strain energy release rate and has units of J/m^2; and K_I is the stress intensity factor, which depends on the nature of loading. For fixed material and loading conditions, the values of G and K_I are fixed at unique values. Here, specific values of fracture toughness, K_c, and corresponding fracture energy, G_c, can be defined as material properties that are independent of the loading conditions. We would like to point out that although G and K_I are also a function of crack velocity, we are not taking that into consideration here. Interested readers can refer to previous literatures to learn more about this (31) (34). When the process zone has a considerable size, we can no longer ignore the nonlinear processes of the energy flow at the crack tip during crack opening. The distribution of stress field near the crack tip becomes important. In this case, the LEFM fails to justify the large amount of fracture toughness of the material, and we treat these materials under elastic plastic fracture mechanics (EPFM). The *J*-integral (31) (35) (36) and cohesive zone model (CZM) (37) (38) are the two most accurate methods to determine the toughness of materials where yielding takes place to a large extent. In *J*-integral we calculate the path-independent *J* function, whereas in CZM we measure the nominal stress against crack displacement, δ. In *J*-integral, it is the final value of *J* that is comparative to G ($J_c = G_c$) discussed earlier; in the case of CZM, the area under traction–displacement curve gives you the value of fracture energy (G_c).We do not go into much

details of *J*-integral and CZM as they require complex mathematical equations and are beyond the scope of this chapter. In all cases, we can safely assert that the fracture energy is the ultimate parameter to describe the toughness of a material.

2.3 Fracture Energy of Hyperelastic Materials

When we talk about hyperelastic materials, such as elastomers and hydrogels, there are two main mechanical behaviors that are different from normal elastic materials. First, the deformation of these materials is more of an entropic phenomenon than an enthalpy one: most of the exerted work changes the entropy of the system (aligning and deforming the configuration of polymer chains). This is why hyperelastic materials undergo nonlinear deformation. Second, the strain values at fracture point in these materials are very large. Naturally, the fracture of hyperelastic materials does not follow the Griffith theory, which is based on linear elasticity of materials. However, the concept of fracture energy during crack propagation still prevails; that is, the larger the fracture energy is, the tougher that elastomer/hydrogel is (39) (40).

To discuss the fracture energy of hydrogels, we will follow the treatment as carried out by Zhao *et al*. Here, we also assume the fracture energy (Γ) to be comprised of two terms: (i) intrinsic fracture energy (Γ_0), that is, the energy required to rupture the chain bonds at the crack bridge, and (ii) fracture energy in the form of mechanical energy dissipation in the process zone (Γ_P):

$$\Gamma = \Gamma_0 + \Gamma_P \qquad 2.4$$

2.3.1 Intrinsic Fracture Energy

Intrinsic fracture energy of hydrogel results due to the rupture of bonds of polymer chain segments present at the crack bridge. In 1967, Lake and Thomas proposed their famous theory regarding the fracture energy of the elastomers (41). The theory was motivated by unexpected large fracture energy observed in natural rubber when compared with the energy required to

dissociate bonds across a crack plane. The theory assumes that if you consider a polymer chain segment across the crack bridge during crack propagation in an elastomer, then all the bonds present in that chain segment are equally stretched to the extent of breakage (Figure 2.1). In this scenario, the crack advances through the breakage of chains, while the event is stochastic. Here, the energy associated with crack propagation is equal to the energy required to break all the monomer units present in that chain segment. If n is the number of monomer units present in that chain segment and U is the energy required to rupture a single monomer unit, then, in mathematical terms, the energy required to break all the bonds will become nU. Now if the number of chains present per unit area of the crack surface is Σ_0., then the intrinsic fracture energy (Γ_0) will be given by

$$\Gamma_0 = \Sigma_0 nU \qquad 2.5$$

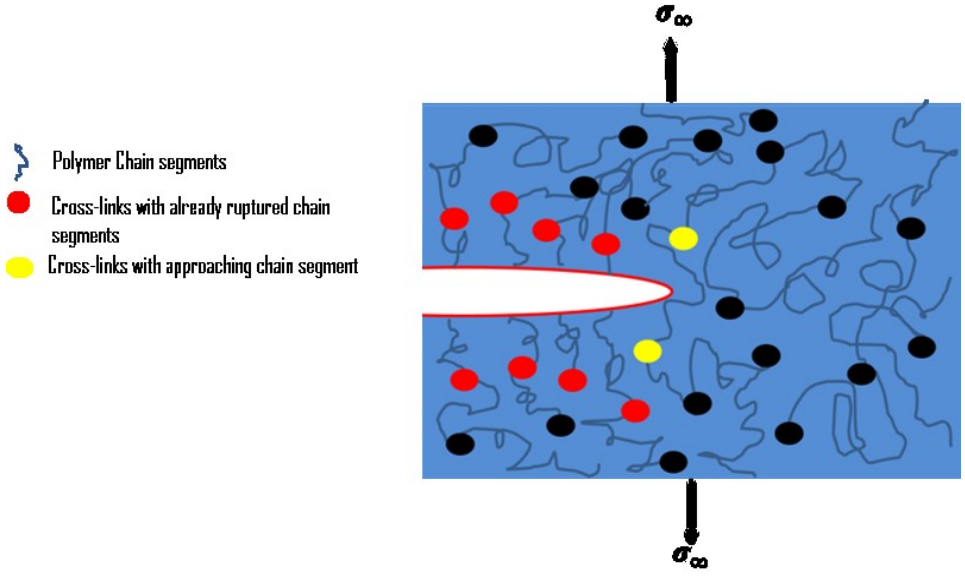

Figure 2.1: Schematic illustration of crack propagation in elastomers based on Lake–Thomas theory.

For hydrogels, the value of Σ_0 is essentially a function of swelling ratio; that is, more swelling implies less number of chains present per unit area. This suggests that at higher swelling ratios, hydrogels have less fracture energy and thus they become more brittle, which may not be true in reality. Moreover, in the aforementioned model, the deformation of neighboring chains in the process zone, which can be a major reason for energy dissipation, is not considered. Therefore, we will show an in-depth consideration of fracture energy in the following section. The other thing we want to point out here is that for a fixed system, such as polymer network with fixed cross-linking density and monomer units, the value of Γ_0 becomes constant. Thus, if we want to increase the toughness of a hydrogel, we need to focus on the second term of equation 2.4.This is the key point to improve the fracture toughness of hydrogels that we will discuss in Section 2.4.

2.3.2 Fracture Energy Dissipation

When crack propagates in hydrogels, large amount of deformation takes place in the polymer chains that surround the ruptured chain segments. This deformation accounts for further increase in the fracture energy of hydrogels (liable for Γ_P) and is thus accountable for the increased fracture toughness. Experimentally, this mechanical energy dissipation is evident in the stress–strain hysteresis of hydrogels, especially at higher strain values (Figure 2.2b). The quantitative analysis of fracture energy is typically carried out with the help of numerical techniques such as finite element method (42) (43) (44) or phase field model (45). Inspired by the treatment of tough ceramics, Zhao (46) recently suggested a physical interpretation of the value of Γ_P. According to Zhao, if we divide the whole process zone in small segments of height, dy (Figure 2.2a), and know the value of energy dissipated per unit volume inside the process zone (w_D), which can easily be obtained by calculating the area of the stress–strain hysteresis loop, the value of Γ_P can be given by following equation:

$$\Gamma_P = 2V \int_0^h w_D \, dy \qquad 2.6$$

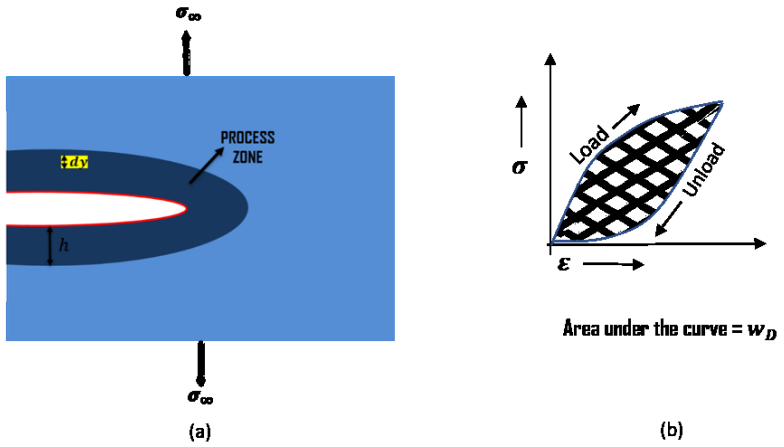

Figure 2.2: (a) Schematic representation of the process zone inside a hyperelastic material. dy and h represent infinitesimal volume element and height of the process zone, respectively. (b) Due to the formation of process zone, loading curve possesses hysteresis loop. Value of w_D can be determined by calculating the area of this hysteresis curve.

where V and h are the volume fraction of hydrogel comprising the process zone and height of the process zone, respectively. The factor of 2 comes due to the inclusion of process zones on both sides of the crack. Later he compared the numerically calculated value of Γ_P with the intrinsic fracture energy of hydrogel (Γ_0, as calculated from Lake–Thomas theory) and found the Γ_P value to be 10 times higher than Γ_0 (46).

Experimental Measurement of Fracture Energy

In order to determine the fracture energy of a material, two samples with same material and size are used. In one of them, a notch is made at one of its edges. This notch must be larger than other possible natural defects present inside the material. Both samples, with and without notch, are loaded under an external force, and the value of the applied stress is increased continuously. The stress value at the point where the notch starts to advance is the critical stress (σ_c). The elastic

energy stored inside the sample, without the notch, corresponding to this stress value, is then calculated (E_c). The fracture energy of the material can then be easily calculated by diving (E_c) with the area of the crack surface (A_c):

$$\Gamma = {}^{E_c}/_{A_c} \qquad 2.7$$

Examples of the testing methods to determine the value of fracture energy include plane shear test, trouser tear test (47), and single edge notch test (48). For all of these tests, the loading conditions change and remain specific; for example, in plane shear test, one of the dimensions of the sample is kept fixed, while the other two dimensions are allowed to change. Thus, in the case of incompressible material, the value of strain in three different dimensions can be given as λ, $1/\lambda$, and 1. Since fracture energy is an intrinsic property of a material, fracture energy calculated by one method must be consistent with the values determined from other methods (9).

2.4 Designing Tough Hydrogels

2.4.1 Fundamental of Designing Tough Hydrogels

Generally, synthetic hydrogels are very brittle in nature due to the absence of mechanical energy dissipation in process zone, that is, noticeably low value of Γ_P. This problem intensifies when there are heterogeneities present inside the polymer network that frequently arises during the gelation process. Due to the presence of inhomogeneity in cross-linking density or in chain length cross-linked points, or the presence of dangling chains and loops, the value of fracture energy can further

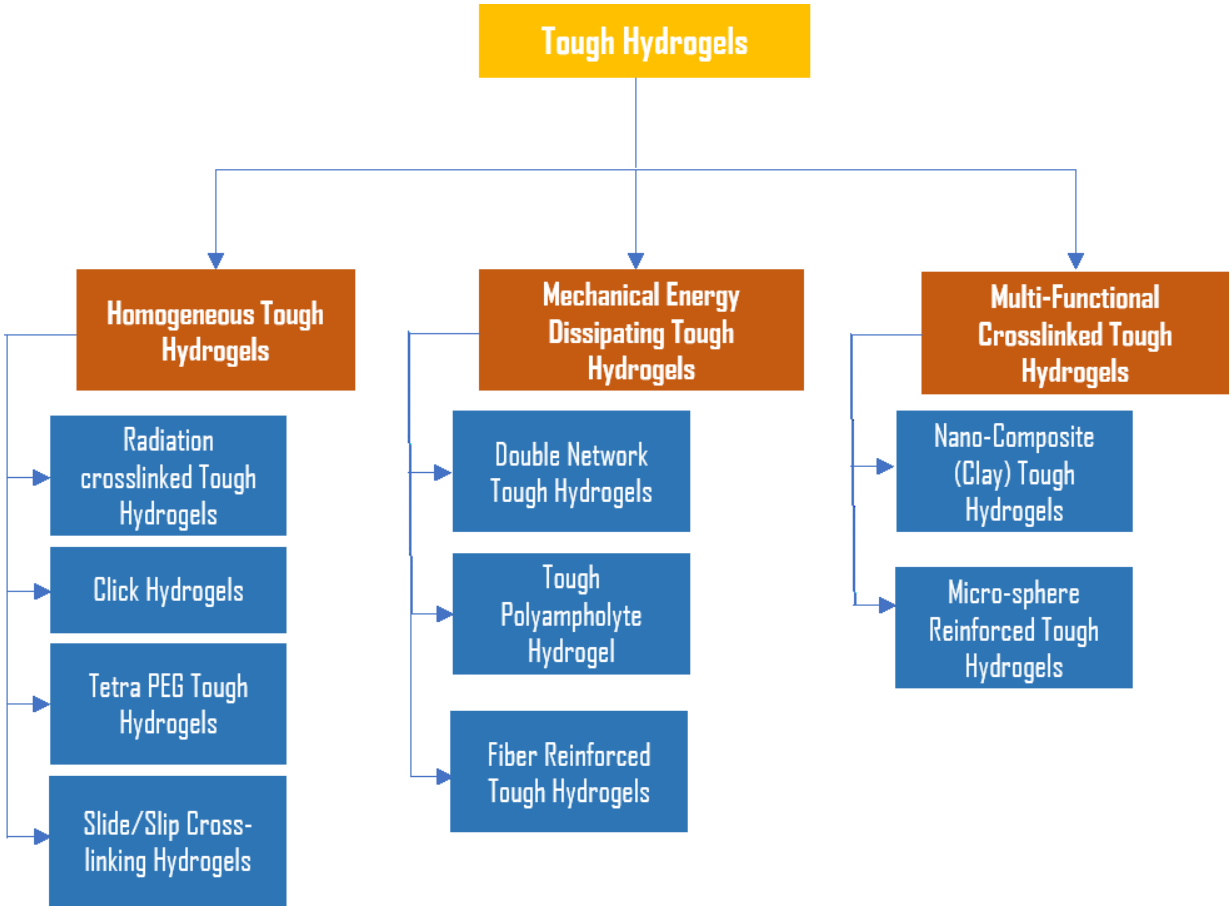

Figure 2.3: Classification of tough hydrogels according to toughening strategies.

decrease (49) (50) (51). Now this phenomenon is quite similar to what we observe during failure of any material: the microstructural defects always play a role as local stress concentrator, leading to a premature failure of the material. This is the reason why actual fracture strength of a material is typically much lower than the calculated theoretical values. Pertaining to the concepts discussed earlier, we have divided the mechanism to synthesize tough hydrogels in three broad categories (Figure 2.3): (i) The first approach to synthesize tough hydrogels is by getting rid of all kinds of heterogeneities in the polymer network, that is, to fabricate homogeneous tough hydrogels. When loading is applied to materials with no internal defects, the stress can be distributed without localization, and hence the premature failure of the material can be prevented. If all kinds of flaws

are eliminated from the microstructure of a hydrogel, then we can at least achieve the fracture energy value equal to the one predicted by Lake–Thomas theory. (ii) The second approach to make hydrogels tough is by introducing a mechanism that dissipates fracture energy during crack propagation. Such mechanisms may include rupture of renewable chemical or physical bonds (double-network (DN) hydrogels) and fracture of fibers or fillers bridging the crack (fiber-reinforced hydrogels). (iii) The third category of tough hydrogels is to incorporate both the mechanisms, that is, uniform stress distribution and mechanical energy dissipation (clay-based nanocomposite (NC) hydrogels). It must be stressed out that the tough hydrogel must recover its original shape and size when external stress is removed. This concept, named resilience, is very crucial to take into consideration because preventing plastic deformation is a crucial concept for material design (46). In addition to the change in material shape, plastic deformation makes hydrogels soft and causes fatigue that leads to poor mechanical properties. Therefore, plastic deformation is not desirable to any extent and should be avoided.

2.4.2 Tough Hydrogels Based on Homogeneous Network

Typically, hydrogels are synthesized by polymerization reaction of water-soluble monomers with a small amount of cross-linker with three or more functionalities. The synthesis method is a key source of heterogeneities in hydrogel. The major reason is the difference in the rate of reaction of monomers and cross-linkers; the reactivity of cross-linkers is typically higher due to the multiple functionalities. Furukawa *et al*. (52) studied these kinds of heterogeneities in polyacrylamide (PAAm) gels by scanning microscope light scattering (SMLS). They found out that during the early stage of hydrogel synthesis, microgels are formed due to higher reactivity of cross-linkers. Once the concentration of the monomers decreases, the microgels start to connect with each other until all the microgels are connected. Thus, there exist two domains within the hydrogels network:

domains with low and high cross-link density. It was also found that the polymer chains between microgel spheres were more entangled when the initial concentration of the monomers was high. This work proved that inhomogeneity exists in typical synthetic hydrogels. The next question to ask is: why toughness decreases with the presence of heterogeneity in polymer network? Naficy *et al*. (53) have given a very reasonable explanation. When a crack initiates in the less cross-linking domain of the hydrogel, the value of Σ_0, chains present per unit area of the crack plane, will be less, and hence, the value of intrinsic fracture energy will be lower (recall the Lake–Thomas theory). If crack initiates in high cross-linked domain, on the other hand, the value of Σ_0 is higher; however, the intrinsic fracture energy will be low because of the low number of monomer units (n) between the two cross-links. Moreover, the highly cross-linked domain will also be very susceptible to the formation of micro-cracks, which are capable of coalescing so as to form a macro-crack. These cracks can easily propagate through less cross-linked domain. This qualitative explanation is supported by the fact that homogeneous hydrogels exhibit more resistance against fracture than heterogeneous hydrogels of same average cross-linking density (54). Demonstrated in the following text are examples to synthesize homogeneous hydrogels that are mechanically superior in terms of toughness.

2.4.2.1 Practicing Radiation Cross-Linking over Chemical Cross-Linking

As discussed earlier, inhomogeneity in polymer network arises due to difference in the chemical reactivity of monomers and comonomers. Cross-linking via radiation can mitigate the inhomogeneity associated with chemical reactivity difference because radiation cross-linking is not dependent on monomer's reactivity and concentration. Moreover, in radiation cross-linking, the radicals form uniformly throughout the volume, and thus, the probability to achieve evenly distributed cross-links in polymer network increases. Norisuye *et al*. (55) synthesized poly(*N*-

isopropylacrylamide) (PNIPAAm) gel via both chemical and γ-radiation cross-linking and studied the microstructure of the two gels under small-angle neutron scattering (SANS). They found out that inhomogeneities present inside chemical gels were very high compared with γ-ray gels. Recently, Wang *et al*. (56) have also produced strong PAAm and polyacrylic acid (PAA) gels while using γ-radiation to carry out polymerization and cross-linking.

2.4.2.2 "Click" Hydrogels

Further developments in designing homogeneous hydrogels with high strength and better toughness values came up when Malkoch *et al*. proposed the idea of exploiting "click" chemistry to synthesize poly(ethylene glycol) (PEG)-based hydrogels with well-controlled network (6). They also reported very high values of elongation at break (up to ~1600%) and tensile strength (up to ~2400 kPa). In addition, the mechanical properties of these "click" gels were reported to be a function of the length of PEG chains. Later on, several other scientists have successfully used this approach to achieve controlled and homogeneous hydrogel network structure (57) (58) (59) (60).

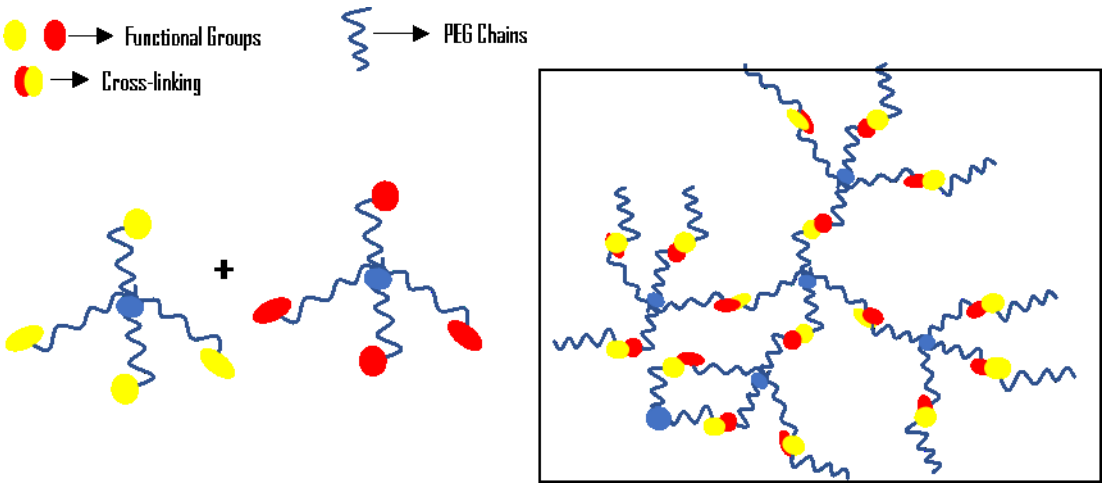

Figure 2.4: Schematic illustration of the structure of tetra-PEG tough hydrogels.

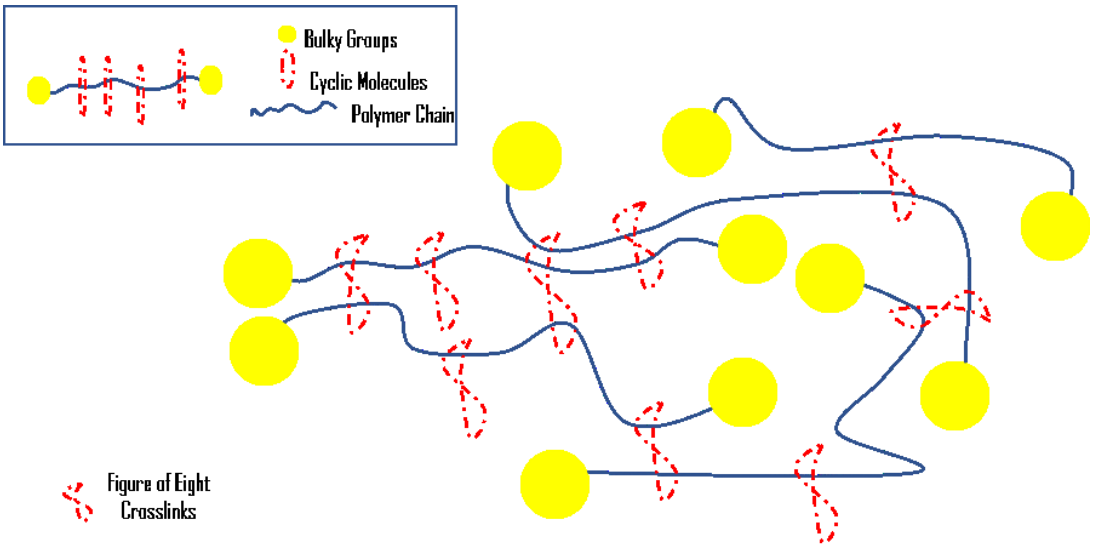

Figure 2.5: Schematic representation of sliding/slipping cross-linkers. Inset shows the basic structure of a polyrotaxane.

2.4.2.3 Tetra-PEG Hydrogels

Going back to the original problem of synthesizing homogeneous hydrogels, Sakai *et al*. (7) identified that defects or inhomogeneity is introduced into hydrogel network due to several asymmetric combinations that can take place during synthesis. These asymmetric combinations can give rise to microstructures with loops or trapped entanglements. If one can decrease the degree of freedom of monomers or reactants involved in the reaction, a uniform network can be achieved by limiting these so-called asymmetric combinations. In order to achieve so, they synthesized PEG-based tetrahedron-like (because of four arms) macro-monomers with different functional groups at the end of their arms as shown in Figure 2.4. These macro-monomers were bulky and symmetrical in nature. When two of those monomers, with different end functional groups (e.g., tetra-amine-terminated PEG and tetra-*N*-hydroxysuccinimide–glutaraldehyde-terminated PEG), are reacted with each other, a cross-coupling reaction takes place to form a homogeneous network (7). These gels are popularly called as tetra-PEG gels. SANS results confirmed the homogeneity of the microstructure of these gels, and it was also found out that heterogeneities are a function of

stoichiometric ratio of the two monomers (61). Maximum homogeneity was achieved when this ratio was 1. These tetra-PEG gels exhibited compressive strength of 2.5MPa (7).

2.4.2.4 Slide/Slip-Ring Hydrogels

Polyrotaxane is, essentially, a system of single polymer chain with many cyclic molecules threaded around it. These cyclic molecules remain bound (to the original polymer chain) because of the presence of bulky groups (caps), attached at the two ends of the chain (Figure 2.5: inset). In 2001, Okumura and Ito (62) introduced a novel polyrotaxane gel based on PEG chains and cyclic α-cyclodextrin (α-CD) molecules. The gel was obtained by simply cross-linking the α-CD molecules. The novel thing about these gels was the ability of cross-links to slide or slip over the polymer chains because, unlike any conventional hydrogel, they are neither chemically nor physically attached to the polymer chains. Because of this reason they are called slide/slip hydrogels. As shown in Figure 2.5, these sliding cross-linkers are called figure-of-eight cross-links. The ability of cross-links to slide imparts remarkable mechanical properties to these gels, as evidenced by high elongation at break (>1000%) and extensive swelling ratio (~400) (62). SANS studies conducted on these hydrogels agreed with the aspect of sliding cross-links under loading (63). It has been suggested that these sliding cross-links act as a pulley when a stress is applied to these hydrogels. The sliding of cross-links distributes external load uniformly throughout the volume of the hydrogel. Thus, stress concentration is mitigated so that the hydrogel can prevent a premature failure.

2.4.3 Tough Hydrogels Based on Mechanical Energy Dissipation

When a crack advances, energy is released and transported to the crack tip; If this energy is sufficient enough to rupture the chemical bonds at the tip of the crack, the crack will propagate. If we devise a mechanism with which this energy is dissipated, the energy transferred to the crack

tip would not be adequate for crack to advance further. This very concept is the basis of designing tough hydrogels based on mechanical energy dissipation. The energy dissipation can be in the form of rupture of physical or covalent bonding in polymer network or fracture of fibers/filler embedded in the matrix of the hydrogel. DN and fiber/filler-reinforced hydrogels fall in this category of tough hydrogels.

2.4.3.1 Double-Network Hydrogels

DN hydrogels were synthesized by Gong *et al*. (64) for the first time in 2003. The DN hydrogels comprise interpenetrating network of the two different polymers that are cross-linked sequentially and independently. These cross-links are generally chemical in nature. The DN hydrogels exhibit a tremendous improvement in the mechanical properties in comparison with the constituting individual network polymers. For example, DN hydrogels with first network of poly(2-acrylamido-2-methyl-1-propanesulfonic acid) (PAMPS) and second network of PAAm can hold stress value of 17.2MPa, in contrast to single-network (SN) PAMPS and PAAm hydrogels, which break at stress values of 0.4 and 0.8MPa, respectively (64).

Synthesis & Basic Features of DN Hydrogels: A typical procedure to synthesize DN hydrogels is two stepped (64) (10) (8). In the early stage, the first network is prepared by carrying out radical polymerization of the monomers, which is followed by cross-linking. The second step involves the swelling of the first network in a solution, containing monomer units of second polymer, and carrying out their polymerization reaction in the first network to obtain DN hydrogel (Figure 2.6). The first network of DN hydrogels is, usually, made up of densely cross-linked strong polyelectrolytes so that they can swell to a very high volume in water. Accordingly, they can accommodate a large amount of second network (up to molar ratio of 20–30). Since the first network swells to a large extent, it remains in a very rigid and brittle state in final hybrid structure

of DN hydrogels. The more rigid the first network becomes, the more susceptible it would be toward the internal fracture. This makes the energy dissipation mechanism very effective and eventually leads to tougher hydrogels. (It may sound awkward, but we will discuss the actual toughening mechanism of these hydrogels shortly.) Now, owing to the charge present on polymer chains, polyelectrolytes are ideal candidate to form the first network of DN hydrogels. Therefore, in most DN hydrogels, the first network is, generally, made up of strong polyelectrolytes such as PAMPS and poly(3-sulfopropyl acrylate potassium salt) (PSAPS). It is notable that neutral polymers, weak polyelectrolytes (65), and physically cross-linked polymers (66) have also been used to form the first network to achieve toughening mechanism anticipated in DN hydrogels. In contrast to the first network, the second network of DN hydrogels is typically made up of loosely cross-linked, neutral, soft, and ductile polymers such as PEG, PAAm, or poly(*N,N*-dimethylacrylamide) (PDMA). It is required that the second network has a very high molecular weight in order to get high toughness values; thus small amount of cross-linker is added to achieve loose cross-linking. Also, molar concentration of the second network should be 20–30 times with respect to the first network in order to set a proper balance between brittleness (from first network) and ductility (from second network) in the final DN hydrogel (8).

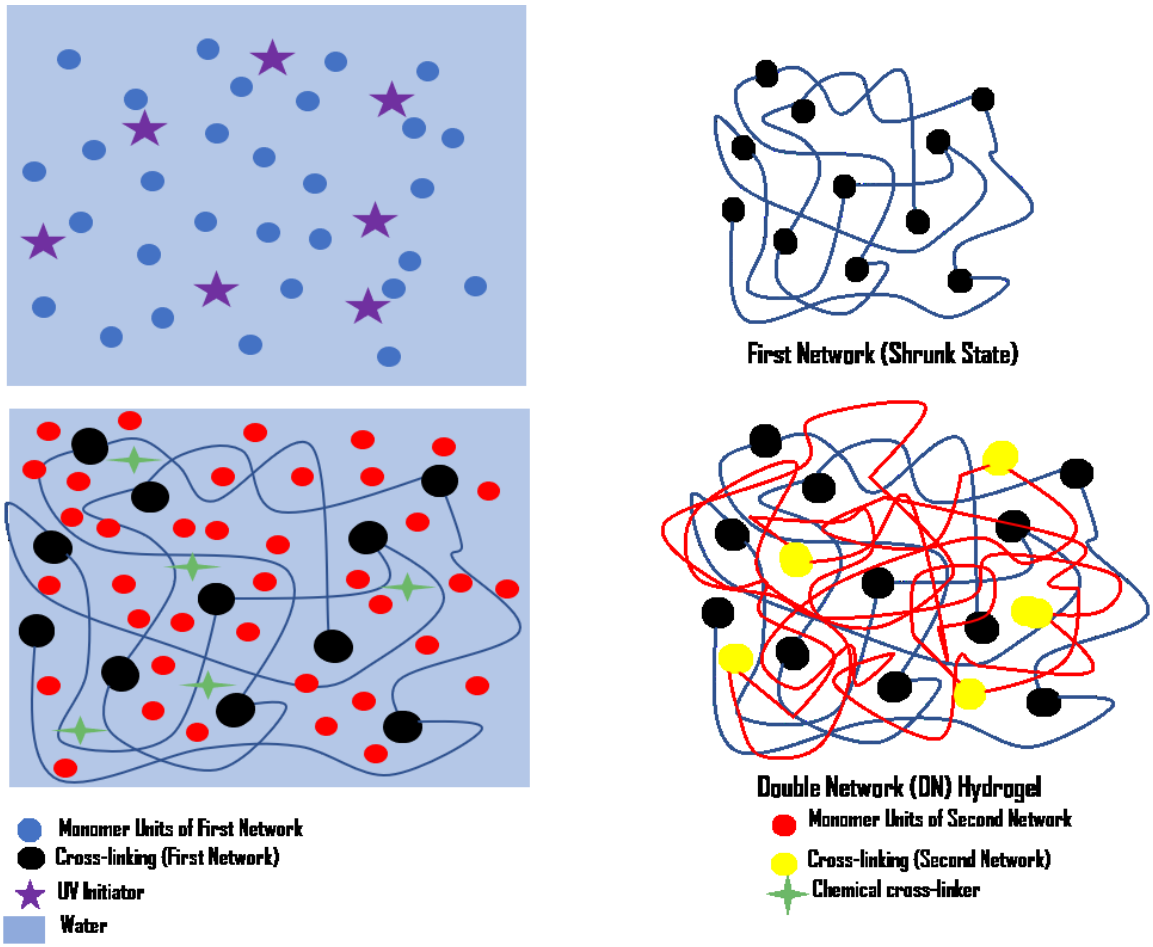

Figure 2.6: Schematic representation of the sequential polymerization of two polymers to synthesize DN hydrogels.

Mechanical Behaviour of DN Hydrogels: During tensile tests, the DN hydrogels exhibit necking phenomenon, that is, formation of narrow zones in the sample (67). The necking zone grows as these hydrogels are further stretched. In the loading curve, this neck propagation shows up in the form of a plateau. It has been found that the stress value corresponding to this plateau, on stress–strain curve, is independent of the strain rate. After neck propagation, the elastic modulus of the gel decreases very sharply; thus, it becomes soft and can stand firm against large elongations. When the load is removed, a significant hysteresis is noticed in the loading curve. This hysteresis aggrandizes with increase in maximum deformation and is not seen in the second loading cycle.

This whole episode implies toward an irreversible change in the structure of DN hydrogels. It has been found out that this change in structure corresponds to the break of the first network into small clusters inside the polymer network. The small clusters of the first network, thus formed, act as cross-linker for large chain segments of the second network. Since these clusters are not chemically bonded to chain segments of the second network, they can slide and act as sliding cross-linker. Slipping or sliding of these clusters, upon deformation, is analogous to slide-ring hydrogels (10). Thus the energy dissipation in DN hydrogels takes place in two forms: (i) due to breakage of the first network and (ii) pulling of polymer chains of the second network.

Toughening mechanism of DN Hydrogels: Theories that are generally used to define the mechanical properties of soft polymeric system such as chain stretching (Lake–Thomas theory) (41) or bulk viscoelasticity (de Gennes theory) (68) cannot explain the large value of fracture toughness of DN hydrogels (69). Alternative theories have been proposed by Okumura (70), Brown (69), and Tanaka (71) to justify the drastic improvement in the mechanical properties of DN hydrogels. Brown's and Tanaka's theories are based on "damage zone model" and successfully explain majority of the structure-dependent mechanical properties of DN hydrogels. In damage zone model, crack propagation comprises two stages. In the first stage, failure of the first network takes place due to its brittle nature owing to high density of cross-linking. Failure involves formation of multiple cracks in the first network, forming a "damaged zone" with very less elastic modulus developing near the primary crack. These micro-cracks are bridged by the second network, which help them stabilize and prevent them to coalesce to form a macro-crack that can readily propagate through the DN hydrogel (72). The second stage involves crack propagation through the second network of DN hydrogel, which will lead to overall failure of the material. In this way, the toughness increases in DN hydrogels, when compared with conventional SN

hydrogels, stems from a large number of non-propagating micro-sized fractures that are required to form a macro-crack that can propagate (53). Experimentally, it has been found that the value of fracture energy increases linearly with the size of damage zone, as predicted by Brown–Tanaka model (73).

Internal micro-fracture of the first network is the prominent form of energy dissipation in DN hydrogels. Thus, while designing these hydrogels, the first network needs to be in maximum swollen state so that it becomes very brittle and rigid, thus making it more susceptible to internal failure. Structural inhomogeneity of the first network also plays a very decisive role in deciding the toughness of DN hydrogels. Radical polymerization leaves substantial amount of voids in the first network. So, when the second network is formed within the first network, these voids are filled and serve as a site for chain entanglements. Once cracks form inside the DN hydrogels, these polymer-filled voids helps in dissipating energy either by viscous dissipation or by polymer chain deformations (74). Experimental study conducted by Nakajima *et al*. showed that the introduction of spherical voids inside the first network (PAMPS) increases the tearing energy of PAMPS–PAAm DN hydrogel by a factor of 2 (75). In order to test the argument, the authors prepared tetra-PEG/PAAm DN hydrogel with very homogeneous first network. They showed that these hydrogels behave in a same manner than any other conventional DN hydrogel (76). This suggests that inhomogeneity in the first network does not introduce a specific toughening or weakening mechanism; rather they simply assist in early internal fracture of the first network.

When the first network of a DN hydrogel fails, it introduces an irreversible structural change to the polymer network. If the first network is based on permanent bonding, DN hydrogels cannot recover and lose their tough mechanical properties. One way to address this issue is forming the first network with reversible cross-linking (physical or ionic bonds). For example, Sun *et al*. (9)

prepared alginate (Ca^{2+})– PAAm DN hydrogels with ionic cross-linking in the first network and covalent cross-linking in the second network. The hydrogel not only showed very high fracture energy (~9000 Jm^{-2}) and high extensibility (17 times of their original length), but they were also able to recover the properties by 74% after the first loading. Chen *et al*. (66), on the other hand, exploited physical cross-linking (hydrogen bonding) to prepare the first network of agar while making agar–PAAm DN hydrogels. Although toughness values for these DN hydrogels were on slightly lower side (~1000 Jm^{-2}), they showed notable recovery after the first loading (65% recovery within 10 min).

2.4.3.2 Tough Polyampholyte Hydrogel

The new class of tough hydrogels that have recently emerged in this category are Polyampholyte (PAm) hydrogels. Polyampholytes are a sub-class of polyelectrolytes where both cationic and anionic repeating groups are present on the same polymer chains. Dr. Gong's group, from Hokkaido University, developed these tough PAm hydrogels by carrying out random co-polymerization of counter charged monomer units around the charge balance point in salt solution (77). The presence of salt ions in the system is essential during the synthesis as it helps in charge screening of the functional groups which prevents the premature precipitation of polymer chains due to inter/intra chain complexation. After the polymerization, the as-prepared PAm hydrogels are dialyzed in DI water to remove all the salt ions present inside the polymer matrix. During the dialysis process, as mobile ions are leached out and the inter/intra chain ion complexation takes place which leads to the deswelling of hydrogels. The resulting hydrogels assume supramolecular structure and are tough, highly stretchable and strongly viscoelastic. It is important to note that, the hydrogels are only formed at high monomer concentration- It is because at low monomer concentration, the polymer chains are small and thus more susceptible towards forming a globular

structure to precipitate or phase separate in spite of salt ions presence. However, at high concentration the long polymer chains entangle each other to prevent the precipitation or phase separation and give a stable hydrogel structure (78).

Tough PAm hydrogels comprise of multiple ionic bonds, formed between oppositely charged functional groups (Figure 2.7). Due to the random distribution of charges, these ionic bonds show a wide distribution of strength. DMA results established that the strength of some of these ionic bonds is as high as ~347 K_BT (K_B- Boltzmann constant) at room temperature, which is comparable to the strength of a covalent bond. However, most of the ionic bonds were found to be much weaker and had lesser strength (77). The toughening mechanism for tough-PAm hydrogels is analogous to that of a DN hydrogel i.e. incorporating a sacrificial structure within the polymer network that breaks as the material is deformed, to absorb large amount of energy, and renders the hydrogel tough as whole. It is suggested that the weaker ionic bonds in PAm hydrogel play the role of sacrificial bonds whereas stronger ionic bonds act as a permanent crosslinkers. As stress is applied to PAm hydrogels, the weaker ionic bonds break and the polymer chains, which are earlier arranged in a globular form, starts to unfold. The former event contributes to the high toughness while the later towards high stretchability of the PAm hydrogels. Once stress is released, the broken ionic bonds reform to reverse back to its original state. The reversible and dynamic nature of weaker bonds also imparts self-healing ability to the PAm hydrogels (79).

From the discussion above it is apparent that ionic bonds are the fundamental constituents of PAm hydrogels which govern bulk of their properties. Thus, any alteration in the structure of these ionic bonds will have direct impact on their properties. For example, it was found that the ionic bonds formed between functional groups with more hydrophobic backbone will overall be much stronger. Since the elasticity of the PAm hydrogel is determined by these stronger ionic bonds, this

will lead to high young's modulus of the hydrogel. However, increase in strength of ionic bonds will cutback their ability to reform at room temperature which will depreciate their ability to self heal.

In comparison with DN hydrogels, PAm hydrogel gives three advantages: (1) Unlike two-step procedure for synthesizing DN hydrogels, PAm hydrogel involves one step polymerization which can be a crucial aspect in scaling up the mass production. (2) The tensile test shows that PAm hydrogels do not leave any residual strain after deformation which makes them fatigue resistant. (3) These PAm hydrogels possess anti-biofouling property and show excellent biocompatibility which makes them an ideal candidate for structural biomaterials (79).

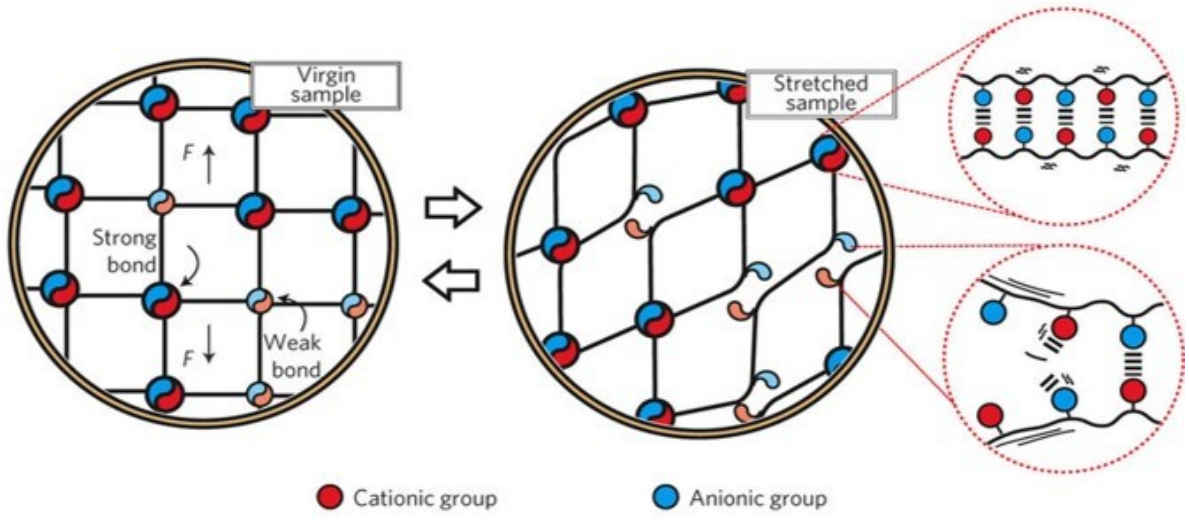

Figure 2.7: Schematic illustration of ionic bonds, of wide strength distribution, formed in polyampholyte hydrogels. The strong ionic bonds act as crosslinker and stay intact while PAm hydrogel is deformed. Weak ionic bonds, on the other hand, break during deformation and absorb energy (Reproduced form the permission of *(77)*.

2.4.3.3 Fiber/Filler-Reinforced Tough Hydrogels

One popular choice to increase the toughness values of rubber is to include other materials such as fibers or fillers into the matrix. The advantage is, in crack propagation, the energy transported to the crack tip has to rupture or pull out the tough fillers that bridge the crack plane in addition to

overcoming the cohesion forces of the matrix. This extra energy required to break or pull out fibers/fillers increases fracture toughness of the material. Several fiber-reinforced hydrogels with remarkable mechanical properties have been successfully produced in the past with the potential application in biomedical field (80) (81) (82).

2.4.4 Multifunctional Cross-Linked Tough Hydrogels

2.4.4.1 Nanocomposite Tough Hydrogels

The origin of multifunctional cross-linked tough hydrogels started with Haraguchi and Takehisa (83), who synthesized NC hydrogels with laponite (composed of silicate nanoplatelets, referred as clay). This NC hydrogel was prepared by simple radical polymerization of water-soluble monomers in the presence of well-dispersed clay nanoparticles (NPs). The initiator molecules are adsorbed onto the NPs due to surface charges. Thus, virtually, the polymerization starts from clay NPs, and, at the end, polymer chains appear to be grafted on top of them. As polymer chains physically get attached with them (non-covalent bonding) and one clay NP can accommodate large number of chains, these clay NPs become multifunctional cross-linking sites within the polymer network.

Microstructure studies showed that each polymer chain can be physically bonded onto multiple clay NPs or multiple times on the same clay NPs. No chemical cross-linker was required to achieve gel state. When chemical cross-linker was used in conjunction with clay NPs, it resulted in brittle hydrogels with low strength (84) (85). It was proposed that the brittleness stems from the introduction of heterogeneities in the polymer network by chemical cross-linking. Schematic structure of the NC hydrogels is shown in Figure 2.8. Here, these NC gels have a unique structure with clay NPs uniformly distributed in the solution and interlinked with each other through flexible polymer chains. Haraguchi *et al*. (86) pointed out that the most important aspect of these NC

hydrogels is the adsorption of polymerization initiators onto the clay NPs as tough gels were not obtained by simply adding the solutions of clay NPs and monomer units (86).

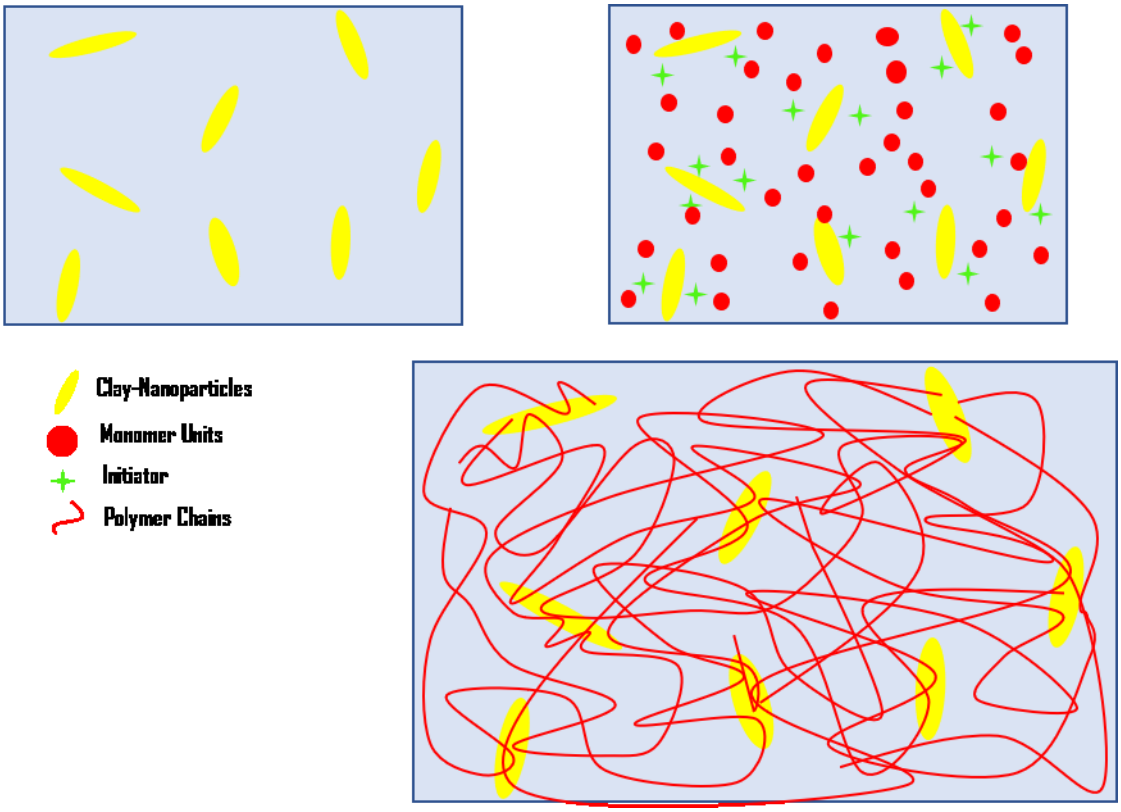

Figure 2.8: Schematic illustration of the structure and synthesis procedure of clay-based nanocomposite tough hydrogels.

Clay NP-based NC hydrogels possess very high values of elastic modulus and elongation (>1000%) at break. Rheology study of the composite hydrogel showed that they are highly viscoelastic in nature (87). Nishida *et al*. have studied the deformation of clay-based NC hydrogels with SANS (88). They found that once load is applied, the clay NPs tend to align with the direction of applied stress. Moreover, since only physical interaction exists between polymer chains, they can very easily peel off from the surface of clay NPs. This brings the structural changes in the polymer network that helps in distributing the stress uniformly. Both of these elements explain the superior mechanical properties of these gels. Both of the mechanisms act to make hydrogels tough, which we have discussed so far: (i) energy dissipation due to the rupture of physical bonds between

the NPs and polymer chains and (ii) structural modification for uniform distribution of stress. There are two features that help these hydrogels to remain intact during deformation. Firstly, the large number of polymer chains attached to each clay NP allows the overall structure to remain unaffected even if few of these chains get desorbed/detached from a clay NP. Secondly, physical bonding between the chains and clay NPs can easily be reconnected after detachment. It has been found out that the probability of this reattachment increases with the increase in molecular weight of the chain segments (53).

Since NC gels are extremely viscoelastic in nature, they are very susceptible to plastic deformation. As we mentioned at the start of the discussion on designing tough hydrogels, plastic deformation is highly undesirable. This issue can be addressed by introducing double cross-linking: chemical cross-linking (to maintain the overall structure of the polymer network) and physical cross-linking (to make hydrogels tough). We previously discussed that chemical cross-linking in NC hydrogels would result in inhomogeneity that leads to brittleness. However, Creton *et al*. (89) prepared double cross-linked PDMA–silica NP tough hydrogel composites with slight chemical cross-linking. These samples possess high fracture toughness and compression strength. More importantly, these gels showed negligible residual strain on unloading, that is, recovery of almost 100% (89). Later on, Gaharwar *et al*. (90) also proposed similar kind of results for tough poly(ethylene glycol) diacrylate (PEG-DA)/laponite-based NC hydrogels. Again, it was claimed that the chemical cross-linking forms elastic network and physical interaction between laponite NPs and polymer chains imparts viscoelastic property to the hydrogels, which is accountable for their high toughness values. The authors also synthesized double cross-linked (chemical and physical) PEG-DA-based NC hydrogels with charged hydroxyapatite NPs and exhibited very high elongation at break (2000%) and fracture stress (1MPa) (91). Functionalized graphene sheets have

also been successfully used to synthesize NC tough hydrogels (92). Here, graphene sheets are irradiated with 60Co γ-rays to generate peroxide functionalities on their surface. These peroxide groups on graphene act as initiators for polymerization reaction and multifunctional cross-linking sites for polymer networks. The hydrogels were found to be extremely resilient and extensible (92). It is worth mentioning here that the physical interactions that allow high toughness values to the NC hydrogels are specific to the particular pair of polymer and NP. Therefore, we might not obtain NC-induced toughness enhancement for two different polymers. Lin *et al*. (93), for example, prepared NC hydrogels based on PDMA and PAAm using silica NPs. Tough hydrogels were obtained in the case of PDMA-based NC hydrogels, and the effect on mechanical properties was negligible for PAAm–silica hybrid hydrogels. It was proposed that since PAAm does not adsorb on silica NP, the physical cross-linking would not occur and hence the resultant gels would not be tough (93).

Numerous studies have been conducted on the NC tough hydrogels; however, the understanding of physics behind all the mechanisms is still highly speculative. A concrete theory to explain the significantly enhanced mechanical properties is yet to be developed. Nevertheless, these NC hydrogels give us an effective option to increase the toughness of hydrogels. This mechanism can also be implemented in conjunction with other mechanisms, which we have discussed so far, to further increase their fracture toughness. For example, Wang *et al*. incorporated silica NPs in DN hydrogels with very high compressive strength (20MPa) and fracture stress value (73MPa) (94).

2.4.4.2 Microsphere-Reinforced Tough Hydrogels

Huang *et al*. (95) suggested that, in conventional hydrogels, the load is distributed to very few chains surrounding the ruptured chain segment when a polymer chain breaks under extension. Now, under extra load, these chains also break, and this operation continues, which, eventually,

leads to the formation of macro-cracks or voids inside the material and causes bulk failure. If this load distribution occurs to a larger volume, that is, if load is distributed to large number of polymer chains, the macro-crack formation can be avoided. Multifunctional cross-linking in polymer network can allow the redistribution of load and hence bestow high fracture toughness to hydrogels. In the case of NC hydrogels, physical bonding between multi-cross-linking sites and polymer chains may not be necessary to achieve higher toughness. In order to support to the idea, Huang *et al*. (95) prepared macromolecular microspheres of styrene, acrylic acid, and butyl acrylate with "active surfaces" of peroxide functionalities, formed by irradiating the microspheres with 60Co γ-rays in the presence of oxygen. These microspheres were then used as initiator and multifunctional cross-linkers to carry out polymerization of acrylic acid monomers. The primary difference between the resultant hybrid hydrogels, in comparison with NC hydrogels, was the presence of covalent bonds between polymer chains and microspheres, which act as multifunctional cross-linkers (Figure 2.9). These hydrogels could sustain the stress of 10.2MPa without fracture, which supports the previous interpretation. Furthermore, Xu *et al*. (96) used core–shell microgels with core made up of cross-linked PNIPAAm and shell of poly (vinyl amine) (PVAm). These microgels were treated with potassium persulfate (KPS) to generate free radicals on amine functional groups in PVAm. The hydrogels thus produced had very high compressive strength (17–30MPa) and showed rapid volume change in response to the change in pH. Due to superior mechanical properties and fast response rate, they are very attractive to be used as substitutive materials for articular cartilage (96). Meid *et al*. (97) also reported PAAm gels with very high mechanical properties by incorporating microgels of PNIPAAm into the matrix of PAAm. Unlike other microsphere-reinforced tough hydrogels discussed so far, a physical

interaction exists between the two polymers, which imparts enhanced mechanical properties (97). Hu *et al*. (98) synthesized microgel-reinforced composite hydrogels with microgels composed of

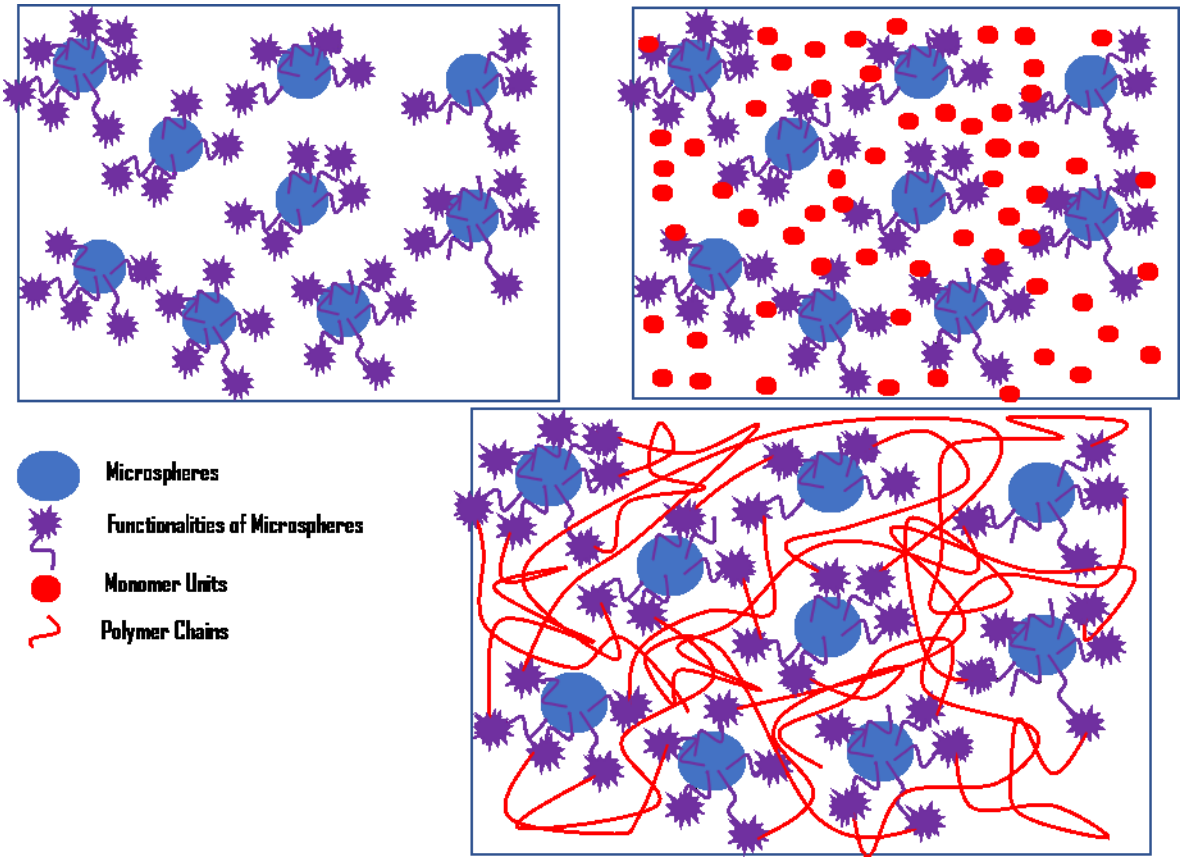

Figure 2.9: Schematic representation of synthesis of microsphere-reinforced tough hydrogels. Unlike NC tough hydrogels, functionalities on microspheres act as both cross-linkers and initiators. In addition, the cross-linking bond between polymer chains and microspheres is covalent in nature.

DN with loosely cross-linked PAAm and highly cross-linked poly (2-acrylamido-2-methylpropanesulfonic sodium) (PNaAMPS). Mechanical properties of these hydrogels were found to be comparable with the DN gels prepared by the same group and claimed to have the potential application for usage in biomedical field.

2.5 Summary

In this chapter, we have attempted to develop physical idea of the different approaches that have been attempted to render hydrogels tough. We started by introducing the concept of fracture

toughness of materials and how it is associated with their fracture energy. Next, we discussed the two elements constituting the fracture energy in hyper-elastic materials i.e. intrinsic fracture energy and mechanical energy dissipation in process zone. Based on which of these elements is targeted to improve the mechanical toughness, we categorized tough hydrogels in three different classes and independently considered the physical origin of toughness for all of them.

Chapter 3. Effect of Dialysis on Conductivity and Mechanical Properties of Tough Polyampholyte Hydrogels

3.1 Introduction

Due to their unique properties that combine the merits of solid and liquid state electrolytes, gel polymer electrolytes (GPEs) have gained a special status in the field of energy storage devices (ESDs). GPEs possess higher conductivity in comparison to solid state electrolytes (99) (100) (101). Moreover, gel formation makes ESDs compact while preventing electrolyte leakage and corrosion which are problems of aqueous electrolytes (21) (102). Ionic conductivity and mechanical robustness are the two key properties that justify the efficacy of a given GPE: The ionic conductivity of GPE affects the equivalent series resistance (ESR) and hence affect power density and specific capacitance of the ESD (103) (104). Mechanical robustness is vital to bear the mechanical load and preserve the structural integrity of the device (26). For GPEs, these two properties follow an inverse relation with one another (105) (106): for example, the family of polyvinyl alcohol (PVA) based hydrogels, a predominant choice among polymeric GPEs, becomes very weak due to the disruption of hydrogen bonding when salt ions are introduced to its polymeric network, whereas such ions are necessary for high conductivity (107). Thus, it is essential to achieve the balance between the two when optimizing a GPE.

Lately, polyampholyte (including polyzwitterionic) hydrogels have been suggested as a potential GPE material in ESDs (101) (108) (109) due to their high-water retention ability and anti-polyelectrolyte effect i.e. they swell more in aqueous solutions with added salts instead of collapsing like ordinary polyelectrolytes (110). Further, PAm hydrogels posses charged species and strong polar groups on their polymer chains which imparts self healing ability and good

adhesion onto contacting surfaces, such as porous electrodes in ESDs. These reasons render PAm hydrogels to be an attractive choice for GPE for ESDs. In Peng et al.'s recent study, (108) graphene-based solid-state supercapacitor employed used polyzwitterionic hydrogels as GPE, whose high-water retention ability and formation of special ion migration channels lead to high conductivity which aided in improving rate capacity and efficiency of their ESDs. In a related topic, Lee et al reported ionic conductivity of polyzwitterionic hydrogels better than various polycationic, polyanionic & neutral hydrogels at high salt concentrations (109).

Our group recently used tough polyampholyte (PAm) hydrogel (a random copolymer system; non-zwitterionic) as a GPE for biochar-based supercapacitors (111). In this study, the ESD exhibited excellent specific capacitance at low temperatures, such as –30 °C, owing to disrupted ice formation and to enhanced water molecule mobility (112). The mechanical integrity of this tough polyampholyte hydrogel, first invented by Gong and co-workers (77), is a result of inter/intra chain ionic complexes with a wide range of bond strengths formed between random clusters of counter charged monomer units. Due to their high toughness, antifouling properties and biocompatibility, this hydrogel has been suggested as a promising candidate for structural biomaterials (77).

Upon dialyzing them in different salt solutions to fully swollen states, we have found that the ionic conductivities and mechanical properties of our PAm GPEs are superior to various PVA-based hydrogels reported in literature (Table 3.1). When salt ions are introduced into the matrix of PAm hydrogels, the weak ionic complexes break to promote the uptake of electrolyte ions into the polymer matrix which increases the ionic conductivity. Meanwhile, the strong ionic complexes stay intact to maintain relatively good mechanical properties. Considering the series of advantages over PVA based hydrogels, as described above, these tough PAm hydrogels can be a promising

candidate for GPE. The strength of ionic complexes in PAm hydrogels is, however, subjective to the natures and strengths of the constituting ions in the salt solutions. It implies that the ionic conductivity and mechanical robustness of a given PAm hydrogel will vary with the species and concentrations of its containing salt solutions. Motivated by these observations, we have carried out a series of experiments to understand the effect of specific ions on the electrical and mechanical properties of PAm hydrogels. This study aims to provide insights in designing an optimized GPE based on PAm hydrogels. In a broader context, understanding the behavior of PAm hydrogels in various ionic media has direct implications in biomedical and in maritime applications of these hydrogels such as bioelectronics, neural tissue engineering, and anti-biofouling coatings, where the effect of surrounding salt ions is a crucial parameter (109).

Table 3.1: Comparison of reported values of ionic conductivity and mechanical properties of various PVA -based hydrogel electrolytes

Hydrogel Electrolyte	Ionic Conductivity (mS/cm)	Concentration of Salt	G'/Y/UTS	Reference
PVA/potassium Borate/KCl	1.02	0.9 M	-	(113)
PVA/KOH/KI	12.73	-	-	(100)
PVA-gPAA-KCl	41	1 M	UTS= 5.82 kPa	(114)
PVA-LiCl	7.5	2 M	G'= 3 kPa	(108)
PVA-$LiClO_4$	48	1 M	Viscous State	(102)
PVA/SA/NaCl (SA-Sodium Alginate)	.0362	Saturated Solution	Y = 550 kPa	(115)
PVA-H_3PO_4	3.4	-	Y ~ 1 MPa	(116)
PAm-KCl	36.01	1M	Y= 37.8 kPa	This Work

3.2 Experimental Section

3.2.1 Materials

Sodium 4-vinylbenzenesulfonate (NaSS; anionic monomer), [3-(methacryloylamino)propyl] trimethylammonium chloride (MPTC; cationic monomer), 2-hydroxy-4′-(2-hydroxyethoxy) -2-methylpropiophenone (photoinitiator), N,N′-Methylenebis(acrylamide) (MBAA; crosslinker), sodium chloride (NaCl), potassium chloride (KCl), lithium chloride (LiCl), ammonium chloride (NH_4Cl), calcium chloride ($CaCl_2$), magnesium chloride ($MgCl_2$), sodium sulfate (Na_2SO_4), sodium nitrate ($NaNO_3$), sodium perchlorate ($NaClO_4$), sodium phosphate dibasic (Na_2HPO_4) were all purchased from Sigma-Aldrich and used as received.

3.2.2 Polyampholyte (PAm) Hydrogel Synthesis

For PAm hydrogel synthesis, we followed the protocol developed by Gong and co-workers (77). Briefly, a symmetric mixture of NaSS and MPTC were added and mixed together in 0.5 M NaCl solution; the concentration of both charged monomers (anionic & cationic) in the final solution was 1M. The amount of photoinitiator added was 0.1 mole% of the total monomers while crosslinker amount was set at 0.3 mole % of the total monomers. This solution was then purged with nitrogen gas for 15 minutes and then injected in between two glass slides separated by a 1mm silicone spacer. The whole set up was placed in UV chamber to carry out the random free radical polymerization for 8 hours (UV broadband lamp with a maximum peak at 365 nm with an intensity of 22 mW cm^{-2}; Jelight UVO-Cleaner Model-342, USA). The as-prepared PAm hydrogel was then dialyzed in deionized water (DIW) to remove all the counterions for 7 days. The water was changed everyday for complete removal of counterions from the hydrogel.

3.2.3 Swelling Studies

The DIW dialyzed PAm hydrogel was cut into small pieces of 1 × 1cm^2 cross-area and each piece was dipped into electrolyte solutions of different salts with various ranges of concentrations. They were immersed for two weeks to reach equilibria. The electrolyte solutions were changed every two days to negate any effect caused by the local change in concentration of the electrolyte in vicinity of the hydrogel. Swelling capacity factor (Q) was defined as the ratio of hydrogel's swelling equilibrium volume in electrolyte solutions (V) and water (V_0): $Q = {}^{V}/_{V_0}$. All the dimensions of hydrogel samples were measured three times using a digital Vernier caliper (MITUTOYO) and their average values were used for further calculations. Three different samples were undertaken for each electrolyte solution and their average values were calculated. The standard deviation across three samples was presented in form of error bars

3.2.4 Ionic Conductivity Calculations

Ionic conductivity of the equilibrated PAm hydrogels was measured by electrochemical impedance spectroscopy (EIS, PGSTAT302N, Metrohm Autolab, Netherlands) with a two-electrode configuration (working & counter electrode). After swelling measurements, the hydrogel samples were sandwiched between two stainless steel electrodes (MTI CORPORATION USA). The EIS measurements were carried out in a frequency range of 0.1 Hz to 100 KHz with an open circuit potential mode using AC excitation voltage of 10 mV. The impedance spectroscopic data was fitted with equivalent circuit model using AUTOLAB software to extract various electrochemical parameters. We used Randles circuit model for fitting as it provided the best fit for physical interpretation of our electrochemical cells. Scheme 3.1 shows the Randels cuicuit model, where R_E corresponds to the resistance towards ion migration inside the electrolyte, R_{CT} is the charge transfer resistance at electrode-electrolyte interface, the Constant Phase Element (CPE)

represents the imperfect electric double layers form at the interface of electrode and surrounding electrolyte, and Z_W is the Warburg coefficient which accounts for the impedance arising from ionic diffusion. The R_E values obtained by this model were then used to calculate the ionic conductivity (κ) by following relation:

$$\kappa = \frac{c}{R_E}$$

where, c is the cell constant as defined by the ratio of thickness to cross-sectional area of the hydrogel electrolyte. Similar to the swelling studies, ionic conductivity was calculated across three different samples, whose average values were taken with the standard deviation represented in the form of error bars.

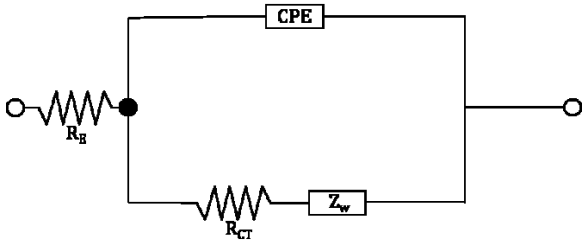

Scheme 3.1: The equivalent block diagram of Randles circuit for impedance data fitting of electrochemical cells

The conductivity of salt solutions (e.g., 1M NaCl solution) at room temperature was double checked by solution conductivity meter (METLER TOLEDO- S75) to validate the accuracy of the conductivity measured by EIS characterizations. To measure the conductivity values, the probe was kept completely immersed into the electrolyte solutions and the measurements was taken after waiting for 5 seconds. Like previous cases, here also we took three conductivity values to extract the averages and the standard deviations. Before changing the electrolyte solution, the probe was completely rinsed with DIW to remove all the adsorbed ions on the probe.

3.2.5 Tensile Test

Engineering stress-strain curve for the PAm hydrogels was carried out using a universal testing machine (INSTRON) with the extension rate of 1mm/sec. The test was conducted on standard dumbbell shaped samples. To prevent the dehydration of hydrogel samples during the test, a thin layer of paraffin oil was applied on their surface. Dimensional measurements of hydrogels samples were carried out with digital Vernier Caliper. In order to calculate Young's modulus, we chose the initial linear region on the stress-strain curve and Young's modulus (Y) was calculated using the relation of Y = (Stress) / (Strain).

3.3 Results & Discussion

Based on their ability to influence the structure of water, salt ions can be categorised into kosmotropes and chaotropes. Kosmotropes are well-hydrated ions which promote ordering of water and hence called "structure-makers". Chaotropes, on the other hand, are poorly-hydrated ions and cause disordering of water as "structure-breakers" (117). The ions with high charge density interacts with water molecules more strongly than water molecules itself, and thus they are capable of overcoming water-water hydrogen bonding between the molecules. Whereas, low charge density ions weakly interact with the water molecules and thus minimally interfere with hydrogen bonding between surrounding water molecules. Figure 3.1(a) categories various common salt ions in kosmotropes and chaotropes. In general, smaller sized or multivalent ions with high charge density fall onto kosmotrope side, while bigger monovalent ions with less charge density on chaotrope side. Although, the ability of ions to influence the water structure in itself cannot explain the behaviour of macromolecules in different ionic media, as been found by recent studies (118) (119), this categorization of ions serves as a good starting point to compare water affinities between the different species of ions in our later discussions.

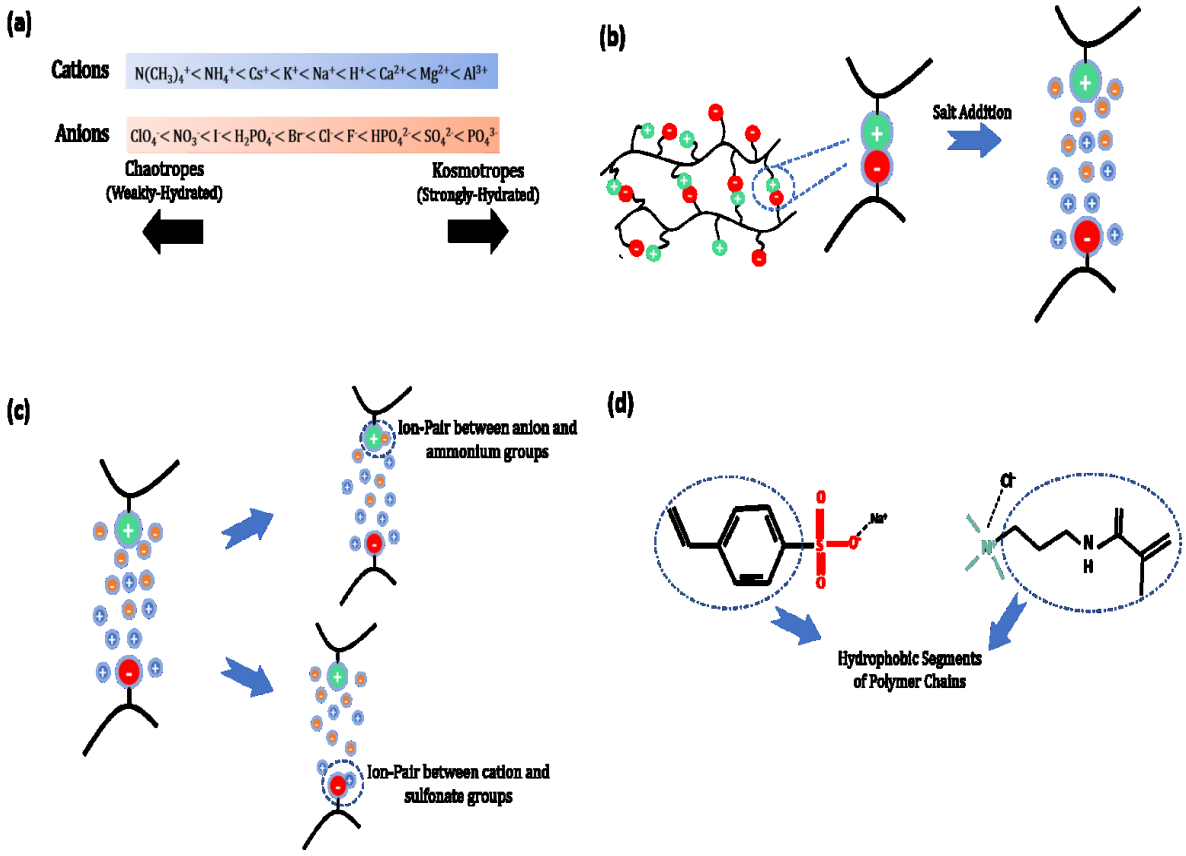

Figure 3.1: (a) Categorization of various cations and anions into chaotropes and kosmotropes. As the charge density of ions increases, their ability to influence the structure of water also increases. Schematic illustrations for (b) charge screening effect by salt ions that leads to a breakup of Coulombic bonding between an anion and a cation in a PAm matrix chain and (c) ion-pair formation between PAm's charged functional groups and a specific foreign ion, which also lead to a breakup of the ionic bonding between the functional groups in the PAm matrix. (d) The ions interfere with the hydration layer surrounding the hydrophobic segments of polymer chains by either increasing or decreasing the surface tension at polymer-water interface.

In order to predict the effect of salt ions on electrical and mechanical properties of tough polyampholyte hydrogels, it is important to understand the nature of interactions that the salt ions will have with functional groups in the matrix polymer and with the water molecules that interact with the PAm chains. Such interactions are termed as salt specific effects. The previous studies of the salt specific effects on hydrogels (119) (120) (121) and polyzwitterionic brushes (122) (123) (124) (125) classify the interactions in three categories: charge screening, ion-pair formation, and ion interference with the hydration layer.

The first category is the charge screening of the functional groups by the background salt ions (Figure 3.1(b)), which weakens the inter- and intra-chain electrostatic attraction between counter-charged functional groups, leading to a breaking of the ionic complexes between the functional groups. Since these ionic complexes essentially act as crosslinkers in tough PAm hydrogels, the breakage of the complexes leads to a decrease of crosslinking density, thus the hydrogel swells and the electrolyte uptake in the hydrogel increases. Debye length (λ_D) is an important parameter to measure the extent of charge screening in electrolyte solutions (126). Low and high values of λ_D correlate to the screening of electrical potential over longer and shorter distances, respectively. According to Debye-Huckel theory, $\lambda_D$can be expressed by:

$$\lambda_D = \sqrt{\frac{\varepsilon_0 \varepsilon_r K_B T}{e^2 \sum_i \rho_i^B z_i^2}} \qquad 3.1$$

where, ε_0 is the vacuum permittivity, ε_r is the relative permittivity of the medium, K_B is the Boltzmann constant, T is the absolute temperature, and ρ_i^B and z_i are the bulk concentration and valency of the ion type, respectively.

The second category is the formation of ion-pairs between the functional groups and salt ions (Figure 3.1(c)). The formation of such ion-pairs perturbs the local charge neutrality of the PAm hydrogels, leading to a local electrostatic repulsion that results in a swelling of the hydrogel (125) (122). The ability to form these ion-pairs is dependent on the nature of ions. In his empirical law of matching water affinity, Collins proposed that the ion-pair formation is energetically favored if both ions possess similar water affinities (127). In our PAm system, the two functional groups in cationic and anionic monomers, sulfonate and quaternary ammonium, respectively, are poorly hydrated. Thus, they are likely to form ion pairs with respective counter-ions that are chaotropic

(125) (128). To distinguish the effect of anions and cations, we have used Na^+ and Cl^- ions as reference in our study because both ions are neither strong chaotrope nor kosmotrope (125). Thus, they have weak tendency to form ion-pairs with the functional groups.

The third category is the interaction of the salt ions with the hydration shell of hydrophobic segments of the polymer chains (Figure 3.1(d)) (119) (129). Different salt ions influence the surface tension at water-polymer interface to different extents. It has been found that kosmotropes, which are strongly hydrated, increase the surface tension of water-polymer interface as they draw water molecules out of the hydration water layer of the polymer (121) (129). As a result, hydrophobic interactions between the matrix chains cause the deswelling of the hydrogel.

Figure 3.2 compare the swelling capacity (Q) of tough PAm hydrogels in the presence of different salt species with three different concentrations for each. The bulk ion concentration (ρ_i^B) increases with higher salt concentrations which consequently enhances charge screening of the functional groups. The number of ion-pair formation and competition for water molecules by ions will also increase with increasing ion concentrations. The fact that Q values increase with increase in salt concentration for all the salts (except for Na_2SO_4 and Na_2HPO_4) signifies that the effects of charge screening and ion-pair formation ordinarily dominates over the hydrophobic interactions in case of tough PAm hydrogels.

Evidently, the effect of the salt's ionic nature on the swelling of PAm hydrogels is much more obvious and significant for anions than cations. For anions, the hydrogel swelling capacity increased following the series $SO_4^{2-} < HPO_4^{2-} < Cl^- < NO_3^- < ClO_4^-$. This trend was in accordance with the known Hofmeister series and can be explained as follows. ClO_4^- is a strong chaotrope, thus it can easily bind with the quaternary ammonium groups in the PAm to form strong ion-pairs that disrupt the local charge neutrality. Therefore, PAm hydrogels show high (Q) values when

ClO_4^- ions are present even at low salt concentrations. For less chaotropic anions in the series, the extent of hydration for anions start to increase. Hence, their tendency to form ion-pairs with quaternary ammonium groups in the PAm decreases. At the same time, the less chaotropic anions tend to draw more water molecules from the vicinity of the PAm chains to promote more hydrophobic interactions. Both effects contribute towards the deswelling of the PAm hydrogels. Finally, strong kosmotropes such as SO_4^{2-} and HPO_4^{2-} exhibit negligible swelling capacity even at high salt concentration of Na_2SO_4 and Na_2HPO_4 respectively. This is because, in the presence of SO_4^{2-} and HPO_4^{2-} ions, the charge screening and disruption of ionic complexes are dominated by the water competing effect (i.e., increased hydrophobic interactions between PAm chains by drawing of water molecules towards kosmotropic ions in the salt). This observation is consistent with previous studies where sulfate ions were reported to dehydrate the grafted polymer chains of polyzwitterionic brushes (122) (123) (125).

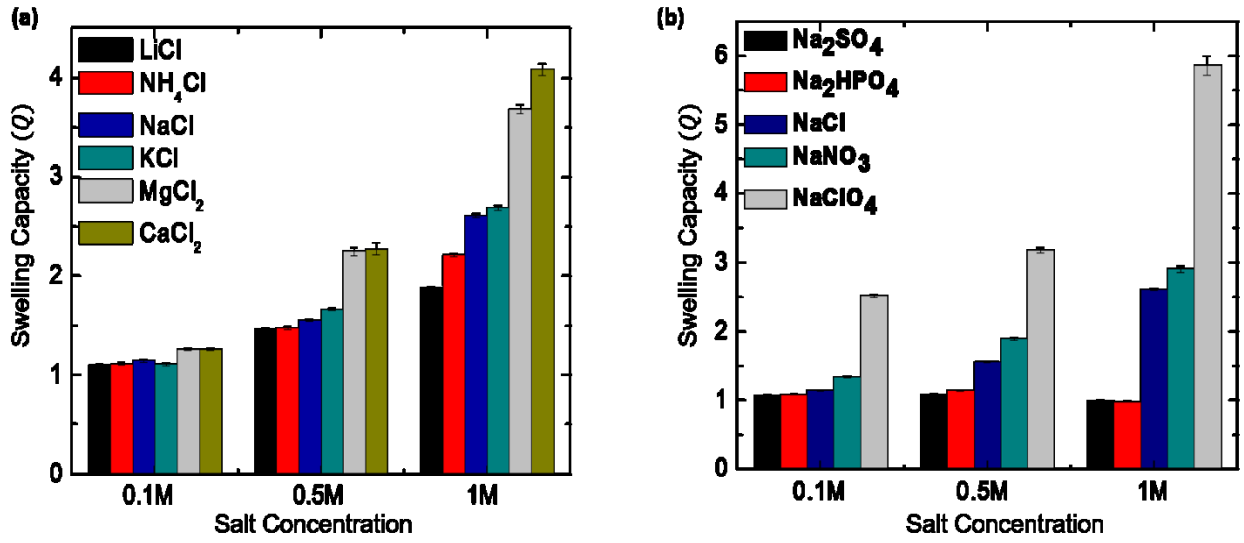

Figure 3.2: Swelling capacity (Q) of tough polyampholyte hydrogels immersed in electrolyte solutions with different (a) cationic species (common anion: Cl^-) and (b) anionic species (common cation: Na^+) at three different salt concentrations. The error bars here represent the standard deviation in Q values.

The trend for cationic species on swelling capacity of hydrogel, however, deviates from the expectations of Hoffmeister effect compared to the case for anionic species. From the discussion above, one would assume that divalent cations (Ca^{2+} and Mg^{2+}) are more kosmotropic and thus will not be able to form ion-pairs with sulfonate groups and eventually will have less swelling capacity in comparison to monovalent cations (Li^+, NH_4^+, Na^+, K^+). However, opposite effect is observed for the hydrogel swelling capacity as we observed the order of $Li^+ < NH_4^+ < Na^+ < K^+ < Mg^{2+} < Ca^{2+}$. One possible reason for this anomaly might be that Ca^{2+} and Mg^{2+} ions, although strongly hydrated, have been reported to show chaotropic behaviour (130) and hence form ion-pairs with sulfonate groups more favorably than monovalent cations. Xu *et al*. (131) also found that the binding affinity of cations with sulfonate groups was maximum for Ca^{2+} ions, followed by K^+, Na^+ and Li^+ ions. Moreover, due to their higher valency ($z = 2$) of cations and higher bulk ion concentration of anions ($(\rho_{Cl}^B)CaCl_2 = 2(\rho_{Cl}^B)NaCl$), the Debye length will be smaller and hence extent of charge screening of functional groups will be more. These factors contribute to the higher Q values for divalent cations. The known Hoffmeister series expects monovalent cations to be arranged as $NH_4^+ > K^+ > Na^+ > Li^+$ on the basis of their chaotropic nature. Except for NH_4^+ions, their relative positions in the order of Q values in Figure 3.1(a) follow the expectation. The reason for the peculiar positioning of NH_4^+ ions is not clear at this moment.

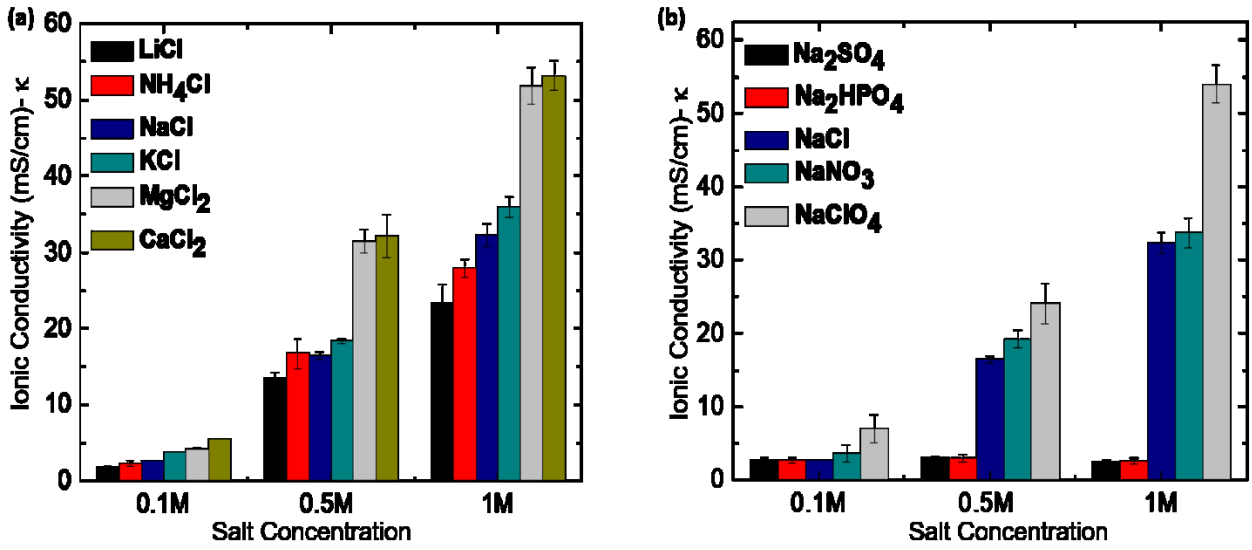

Figure 3.3: Ionic conductivity comparison of polyampholyte hydrogels with electrolyte media of different concentrations and nature. Ion conductivity values for electrolytes with (a) different cations (common anion: Cl^-) and (b) different anions (common cation: Na^+). The error bars represent the standard variation of ionic conductivity across three different samples under identical conditions.

Ionic conductivity of PAm hydrogel samples was measured by carrying out impedance spectroscopy using a potentiostat. For PAm hydrogels completely dialyzed in DIW, the conductivity was .011 mS/cm, which was very similar to the conductivity of DIW (.005 mS/cm). This result confirms that almost all Na^+ and Cl^- counterions, which exist in the constituting monomers thus also exist in the as-cast PAm hydrogel before dialysis, got removed from the hydrogels during the DIW dialysis process. The ionic conductivity of the electrolyte is governed by bulk ion concentration and the mobility of the ions. The ion concentration is a function of salt content in electrolyte and increases with the addition of salt. When salt concentration is constant, the ion mobility in hydrogel increases with water content in the hydrogel (i.e., less PAm matrix content per unit volume in the hydrogel), thus enhances the ionic conductivity (132). Since both factors – higher ion concentration and ionic mobility – ensue more swelling, the ionic conductivity of PAm hydrogels follows the similar trend as Q values of the hydrogels. In other words, the

conductivity of PAm hydrogels among different salt species (Figure 3.3 (a) & (b)) follow the trend of Q values (Figure 3.2 (a) & (b), respectively), irrespective of the molar conductivity of salt ions (Table 3.2).

Table 3.2: Ionic conductivity of various aqueous solutions with various salts at three different concentrations

Salt 0.1M	Conductivity (mS/cm)	Salt 0.5M	Conductivity (mS/cm)	Salt 1M	Conductivity (mS/cm)
LiCl	12.04±.02	LiCl	42.05 ± .07	LiCl	85.85±.16
NH_4Cl	14.30±.05	NH_4Cl	55.75±.08	NH_4Cl	104.71±.37
NaCl	11.18±.06	NaCl	46.15±.08	NaCl	71.99±.28
KCl	13.10±.49	KCl	61.22±.30	KCl	110.91±.95
$MgCl_2$	16.97±.06	$MgCl_2$	66.10±.27	$MgCl_2$	105.25±.45
$CaCl_2$	18.46±.11	$CaCl_2$	72.91±.40	$CaCl_2$	125.54±.46
Na_2SO_4	15.58±.09	Na_2SO_4	60.46±.20	Na_2SO_4	93.44±.23
Na_2HPO_4	15.6±.08	Na_2HPO_4	56.43±.43	Na_2HPO_4	81.22±.65
$NaNO_3$	13.72±.08	$NaNO_3$	41.58±.15	$NaNO_3$	73.16±.21
$NaClO_4$	10.09±.04	$NaClO_4$	43.81±.24	$NaClO_4$	74.86±.35

For same concentration across different salt ions, the bulk ion concentration remains same and thus the difference in conductivity stems from the mobility of ions in the hydrogel. The charged functional groups on polymer chains also play their part in influencing the ionic mobility. Simulation studies have shown that ions near the polymer chains have, on average, lower mobility in comparison to the ones far from the polymer network due to electrostatic attraction (133). Saito

et al. also asserted that the preferential attraction of one counterion to functional groups on the polymer chains reduces its mobility and subsequently benefits the transportation of other counterion by curtailing the chances of two counterions to bump into one another (134). They found that, in overall, this phenomenon leads to high conductivity of the polymer gel electrolyte. As we have discussed above, in PAm hydrogels, the presence of functional groups on polymer chains form ions pairs with electrolyte ions and thus promotes both fast salt dissociation and ionic transportation (109) (135). These can be the two possible explanations for higher conductivity of PAm hydrogels high saline concentration (Table 3.1).

The ionic conductivity in gel polymer electrolytes, which increases with decreasing PAm to water ratio, comes at the expense of their mechanical properties. So, quite expectedly, the Young's modulus of PAm hydrogels decreased with the increase in salt concentration of the electrolyte. The superior mechanical properties in PAm hydrogels arises from the wide distribution of the strengths of ionic complexes that forms between counter charged functional groups in the PAm matrix. As the electrolyte ions are introduced into the polymer matrix, the weak ionic complexes break which leads to hydrogel swelling and electrolyte uptake due to charge screening and ion-pair formation. However, the strong ionic complexes still stay intact, thus reasonably good mechanical properties of the PAm hydrogels can be maintained even at high salt concentration. As the ion concentration inside the hydrogel increased, the Young's modulus decreased and elongation at the break increases. Just like ionic conductivity, the Young's modulus of PAm hydrogels in different ionic media can also be rationalized by their swelling capacity: Salt ions that cause more swelling of PAm hydrogels result in smaller Young's modulus. Except for the case of Na_2SO_4 and Na_2HPO_4, Young's modulus of PAm hydrogels decreases to a large extent compared to its original value (2.06 MPa; after DI water dialysis) when immersed in salt solutions. However,

these values are significantly better than PVA based hydrogel electrolytes with similar ionic conductivity values (Refer Table 3.1).

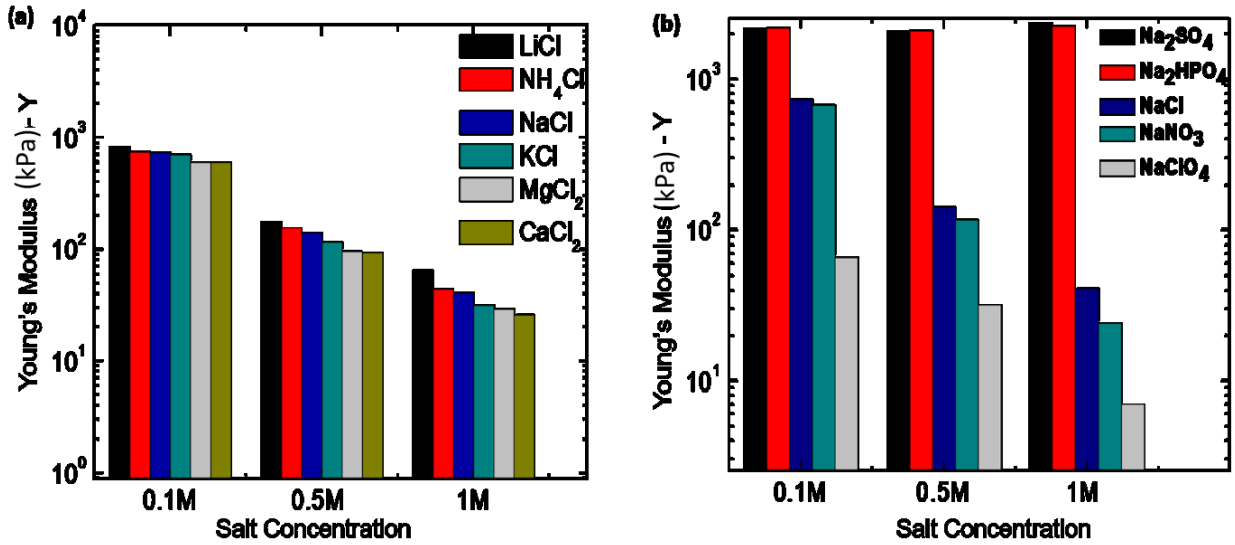

Figure 3.4: Comparison of Young's moduli for polyampholyte hydrogel samples dialyzed in various salt solutions with three different concentrations. Here, (a) cationic species (common anion: Cl^-) and (b) anionic species (common cation: Na^+) were varied. The trend for the Young's moduli of the PAm hydrogel samples followed an inverse relationship with their swelling capacity shown in Figure 3.2.

3.4 Conclusion

The multifunctional features of polyampholyte hydrogels have prompted a surge of interest for their application as gel electrolyte in energy applications. In this work we have carried a systematic investigation on ion-specific behaviour of tough polyampholyte hydrogels. We proposed three different ways in which ions interact with the polymer chains of the hydrogel: (i) Charge screening of the functional groups (ii) formation of ion-pairs between electrolyte ions and charged functional groups, and (iii) influencing the hydrophobic hydration layer of the polymer chains. It was shown that the ability of electrolyte ions to form ion-pairs mostly governs the swelling of PAm hydrogels in electrolyte solutions. Because of their similar water affinities with functional groups, chaotropic ions seemed to form stronger ion-pairs and thus PAm hydrogels had more swelling capacity in

their presence. However, the strong water-competing effect dominates for kosmotropic ions which leads to minimal swelling of the hydrogels in their presence even at high salt concentrations. We have also discussed here about the role of charged functional groups in promoting salt dissociation and fast ion transportation, as they aid in achieving higher conductivity with PAm hydorgels. Just like any other GPE, we observed a trade-off between the ionic conductivity and mechanical properties of PAm hydrogels with ionic nature and ionic strength of the electrolyte. However, even at high salt concentrations the strong ionic complexes of PAm hydrogels stay intact which maintains relatively high Young's modulus of the hydrogel. Due to higher ionic conductivity and better mechanical properties of PAm hydrogels, they can be considered as a straight-forward replacement for PVA based hydrogels as gel electrolyte in energy applications.

Chapter 4. Stretchable Electronic Skin with Colorimetric Temperature Sensing and Capacitive Pressure Sensing Abilities

4.1 Introduction

Skin is a vital interface between our body and the environment that is analogous to a large stretchable sheath embedded with a network of sensors of various functions. For example, skin senses external stimuli from touch, pressure, and temperature which are then analyzed by our nervous system and eventually converted into physiological responses (136) (137). Electronic Skin (e-skin) is an artificial skin mimicry comprising of flexible or stretchable sensor arrays. The e-skins have been developed for decades for biomimetic robots (138) (139) (140) (141), for real-time wireless health monitoring (142) (143) (144) (145) (146) and for human-machine interfaces (147) (148) (149).

The simplest form of an e-skin has a singular functionality for sensing, such as pressure, temperature, strain, or humidity (150) (151) (152) (153) (154) (155) (156) (157). However, practical applications require multi-functionality for e-skin. The most apparent way to realize the multi-functionality is by integrating multiple sensors to a single sensing unit of the e-skin device (158) (159) (160) (161) (162). One factor to consider for multi-functional e-skins is cross-interference problem between the sensors (163) (164) (165) (166). In other words, it is important to ensure each sensor to respond to a specific stimulus without responding to other stimuli. This is achieved by incorporating sensors which do not meddle with each other's sensing mechanisms (167) (144). In addition, the solutions to the cross-interference problem often require sophisticated electronic designs and complicated fabrication procedures (168) (169) (170). Thus, developing

multi-functional e-skins with simple fabrication procedures and sensing mechanisms is an interesting subject for advanced materials and electronics researches.

Tactile and temperature sensing are two important functionalities for human survival as it helps us in navigating our surroundings without injury and in gathering information about objects (171). Extensive studies have been conducted to replicate the sense of human touch using electronic devices for robotic applications. Common transduction modes that have been incorporated for this purpose include piezo-resistivity, capacitance and resistance change and pyroelectricity. Among these modes, the capacitance mode provides advantages of simple device design, low power consumption, and high strain sensitivity (171). In addition to its sensory importance, regular monitoring of local skin temperature can help in detecting various symptoms from illnesses such as breast cancers (172). Thus, having wearable and wireless sensing devices that could determine the temperature of the skin instantly and continuously is desirable. Non-electronic colorimetric sensing has advantages of energy consumption and intuitive perception. With the aid of quantitative image analysis, one can extract exact temperature values from such colorimetric sensors using handheld digital devices, such as smartphones.

Here we report a stretchable bifunctional e-skin based on simple design and facile fabrication steps that can carry out tactile and temperature sensing simultaneously without any detectable cross-interference. For temperature sensing, we embedded thermochromic liquid crystal (el-TLC) in elastomeric matrix as a photonic composite material. While qualitative assessment is available by naked eyes, quantification of the temperature is available by using image analysis from a digital camera at the precision of 0.1 °C. For tactile sensing, we fabricated a multi-pixelated array of capacitive sensors, whereas their transparent electrodes are made from ionically conductive, stretchable, and self adhesive polyampholyte (PAm) hydrogels. The judicial choice of materials

enabled the orthogonality in sensing modes, resulting our e-skin to have no detectable cross-interference problem in the simultaneous measurements of pressure and temperature.

4.2 Results & Discussion

In order to realize bifunctionality, colorimetric sensors has been integrated to electronic devices by using leuco dyes (thermochromic and electrochromic) and TLCs (173) (174). In the current work, we employed a chiral nematic liquid crystal (Chiral Nematic Liquid Crystal Slurry, LCR Hallcrest) dispersed as small microcapsules in elastomeric matrix. This liquid crystalline material has three distinctive phases over ranges of increasing temperatures – from smetic to cholesteric, and finally to nematic phase. While in cholesteric phase, the molecules in TLC are disposed in helical form (175). These helices are uniformly aligned (Figure 4.1 (b)) and reflect the incident light at a certain wavelength, which is represented as a distinguishable color. The reflecting wavelength increases with an increase in the distances between the helices, called helical pitch length. As temperature increases, the pitch length decreases and thus the reflected light undergoes a blue shift. This phenomenon is the basis of quantitative thermal sensing using TLCs. In the other two phases (smetic and nematic), molecules do not exhibit any preferential orientation and thus there is no colorimetric responses to temperatures. In the current work, cholesteric phase exists between 26 and 40 ºC (176). The el-TLC composite was obtained by adding micro-encapsulated TLC slurry into PDMS prepolymer. Figure 4.1 (b) shows the scanning electron microscopy (SEM) image of our thermochromic composite which confirms the size of TLC micro-capsules to be around 1-2 μm. The el-TLC/PDMS composite was instilled and cured into disk-shaped ‘pixels’ with dimensions of 2 mm in diameter and 100 μm in thickness in ‘working-layer’ (Figure 4.2 (a)). This working-layer provides the bi-functionality our e-skin device.

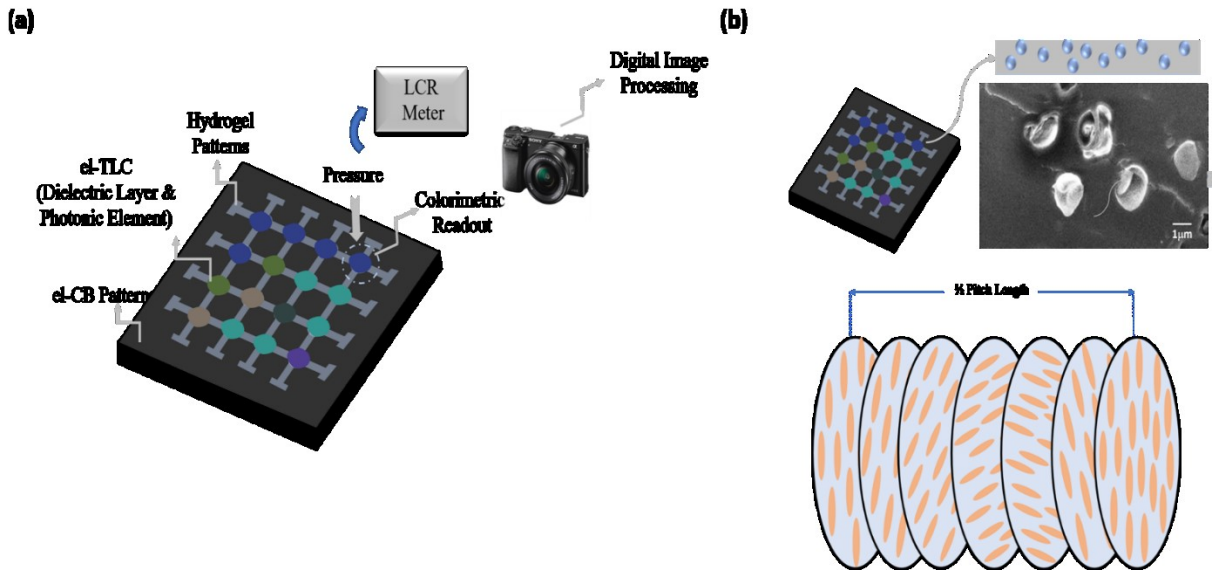

Figure 4.1: (a) Conceptual illustration and operation principle of the bifunctional e-skin device. (b) (top) SEM image of el-TLC composite material and (Bottom) preferential orientation of TLC in cholesteric phase.

For accurate colorimetric evaluation with TLC materials, it is vital to have a non-reflective, dark background which can absorb the incident light and thus prevents the undesirable reflected light. This practice helps in improving signal to noise ratio by enhancing the contrast between the reflected light from TLC material and the background. The background material we fabricated was 300 μm-thick PDMS-carbon black composite (el-CB), which were cut into pre-designed shapes, which give relief for sensory pixels and transparent electrodes that will be explained later, using a CO_2 laser cutter. The working-layer was then sandwiched between two el-CB templates, whereas the alignment between the two el-CB was perpendicular to each other (Figure 4.2 (b)). Stable bonding between these layers was ensured by applying a very thin PDMS-Toluene mortar layer on plasma-treated el-CB templates, followed by curing. This mortar layer essentially functions as an adhesive and provides an effective strategy to bond PDMS based structures (177). The effective light reflection from TLC composite also required to incorporate transparent electrodes which do not obstruct the colorimetric information. Ionically conductive PAm hydrogel was chosen for this

purpose because of their high stretchability and self-adhesive nature, which promotes an intimate contact of the electrodes with dielectric layer and aluminium tapes, which connect the device to power source (not shown here).

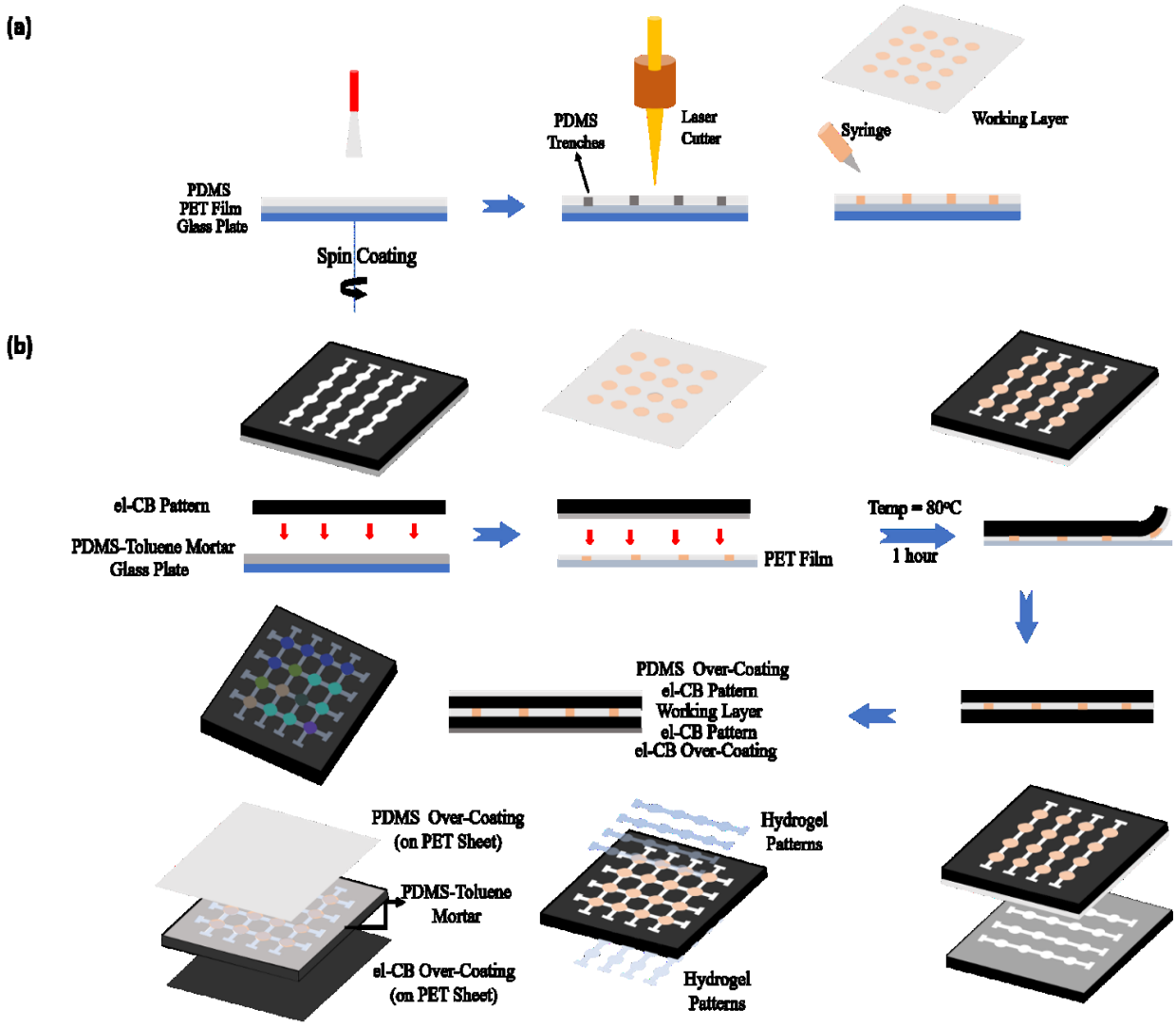

Figure 4.2: Fabrication procedures of (a) the working-layer and (b) the bifunctional e-skin with a five-layer design.

In order to allow patterning of PAm hydrogel layer into the shapes of the sensory pixels and conducting traces, we again used CO_2 laser cutter. These hydrogel patterns serve as transparent electrodes and connecting traces. In order to prevent the hydrogel patterns from drying out, we

applied protective over-coating layers of transparent PDMS on one side and non-patterned el-CB on another side of the e-skin for complete sealing. The non-patterned el-CB over-coating acted as a black background to augment the colorimetric signal from the el-TLC pixels.

In addition to the colorimetric temperature sensitivity, our bifunctional e-skin has 16 independent pixels for tactile sensing based on capacitive measurements. Each cell takes the configuration of a parallel plate capacitor where conductive hydrogel serves as electrodes facing across the dielectric working-layer. When the pressure is applied, the distance between the hydrogel electrodes decreases and the capacitance value increases accordingly. Here, the capacitance of each pixel is tracked independently and multiple touch on the panel can be detected simultaneously. Concurrently, the working-layer reflects any local temperature variation with color change. The change in capacitance, in response to applied pressure, is monitored by LCR meter (BK Precision 894) while colorimetric response to temperature fluctuation is directly visible; quantification of the colorimetric temperature signal was done by image processing by a digital camera (SONY A6000).

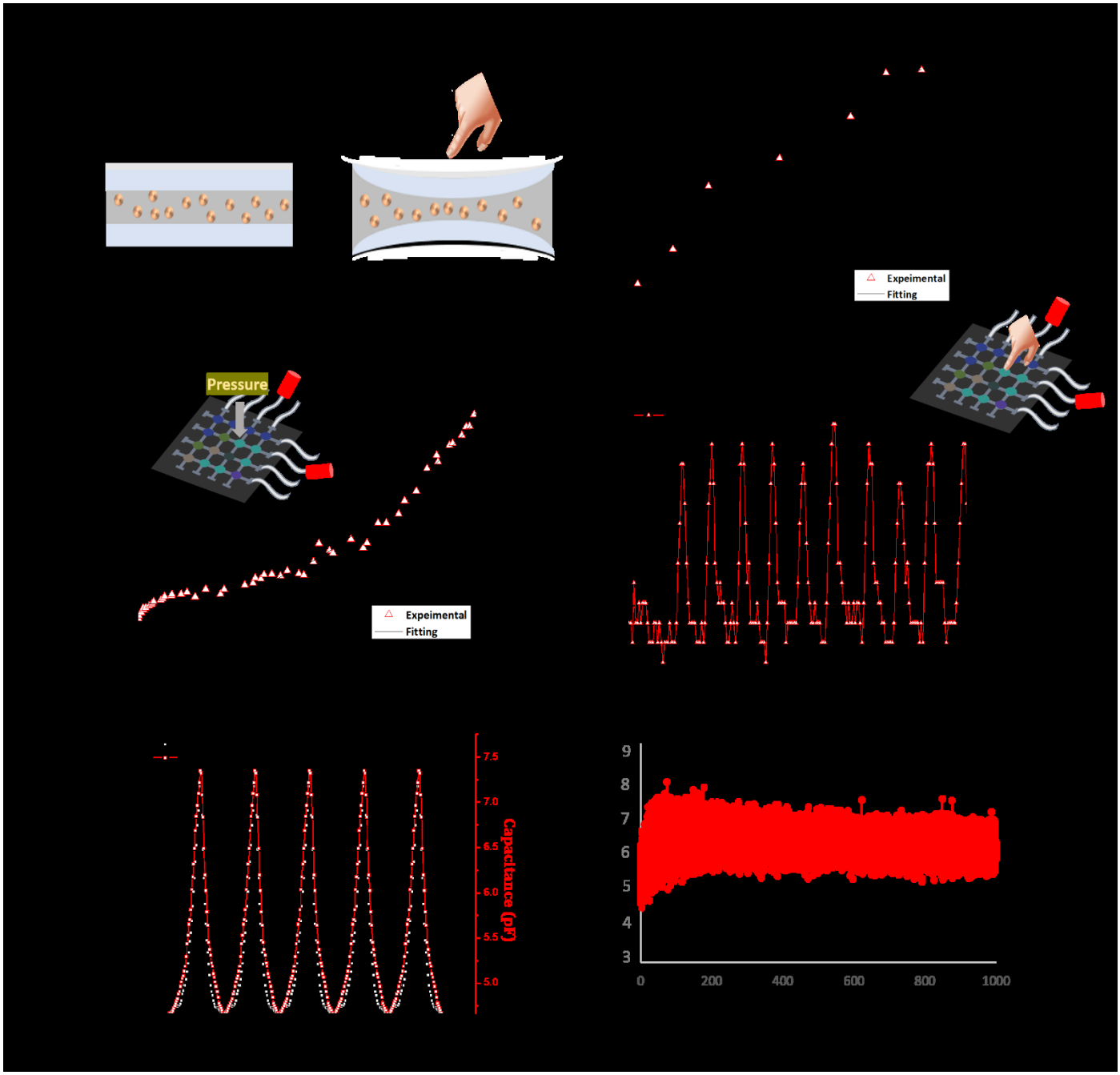

Figure 4.3: (a) Schematic Illustration of deformation of a capacitive sensing pixel upon applied pressure. (b) Variation of dielectric constant of el-TLC composite as a function of added weight fraction of TLC slurry. (c) Capacitance change of tactile sensor pixel with applied pressure. (d) Response of tactile sensor to finger tapping. The applied force during tapping was ~1N. (e) Real time response of tactile sensor to cyclic compressive stress. (f) Variation of sensor's capacitance to compressive stress over 1000 cycles. The frequency of AC signal during all measurements was kept to 1KHz.

A schematic illustration of capacitance sensing for a single tactile sensor pixel is shown in Figure 4.3(a). The applied pressure cause change in dimensions of the sensing pixel by decreasing the thickness ($d_0 \rightarrow d$) of dielectric media between the two electrodes. As a result, there is increase in capacitance value by ΔC, which is given by the following relation:

$$\Delta C = \epsilon_r \epsilon_0 A(\frac{1}{d} - \frac{1}{d_0}) \qquad 4.1$$

where, ε_0 is the vacuum permittivity, ε_r is relative permittivity of the dielectric medium and A is the cross- sectional area. Here, ΔC is a direct function of ε_r and thus measuring the permittivity of the dielectric media is important. We observed that the relative permittivity of our el-TLC composite increases as more wt% of TLC slurry is added to it: ε_r values jumps from ϵ_r= 2.7 (relative permittivity of PDMS) to ϵ_r= 4.2 at 35 wt % of TLC slurry (Figure 4.3(b)). For all the measurements carried out in this study, we used 35 wt% of TLC slurry only. At this composition, the increase in dielectric constant enhances the capacitance change by ~ 1.56 times compared to that of neat PDMS, and so does the pressure sensitivity of our device. Figure 4.3(c) shows the capacitance variation of single sensing pixel in response to the applied pressure (P_{appl}). Here, P_{appl} is defined as applied force divided by the cross-sectional area of the sensing pixel (i.e. 12.56 mm^2). The capacitance increases with applied pressure. In the range of typical weak (50-100 kPa) and normal human touch (150-200 kPa) (178), our sensor maintains a very good sensitivity of 0.011 kPa^{-1}. Our tactile sensing pixel could also sense a gentle tap of a human finger as shown in Figure 4.3(d). The force applied during the tapping was around 1 N. The capacitive response of our device was found to be reliable and reversible. We applied a cyclic pressure of 250 kPa to a sensing pixel at the rate of 0.5mm/min (UniVert mechanical tester, Cell Scale) and the capacitance was recorded

in real time (Figure 4.3(e)). Here, our tactile sensor could withstand 1000 compressing cycles without losing its performance (Figure 4.3(f)).

Figure 4.4(a) contain digital images of a single sensing pixel at different temperatures. The colorimetric response of our el-TLC composite to temperature change is clearly discernible from naked eyes. However, the quantitative analysis requires digital image acquisition and processing. The quantification of temperature is carried out by constructing a hue-temperature calibration curve (175) (179) (180). The hue saturation value (HSV) color space is preferred over red-green-blue (RGB) for TLC materials because the color information in HSV space is stored only in hue component, whereas three separate values are required for RGB space. The hue angle represents the primary color and any change in surrounding lightning conditions only affect the saturation and value components of HSV space. Therefore, the hue angle is a reliable parameter for calibrating colorimetric interpretation of TLC materials.

To obtain the calibration curve for el-TLC composite, we prepared an individual sensing pixel and placed it on top of a Peltier stage (TS102G, Instec Inc.). The temperature of the stage was brought to a certain point. After waiting for 15 seconds to attain thermal equilibrium, digital images of the sample were taken. We used IR camera (Seek Thermal) to confirm that the temperature of stage is same on the pixel. The colorimetric output was obtained by a digital camera, then the images were converted to HSV color space by a custom-made MATLAB program. This practice was carried out three times to obtain data sets from three different samples (Figure 4.4(b)). These datasets were used to fit a five-degree polynomial curve to obtain temperature to hue. The temperature measured from this $T = f(h)$ relation, has an expected uncertainty (ΔT), which can be given by:

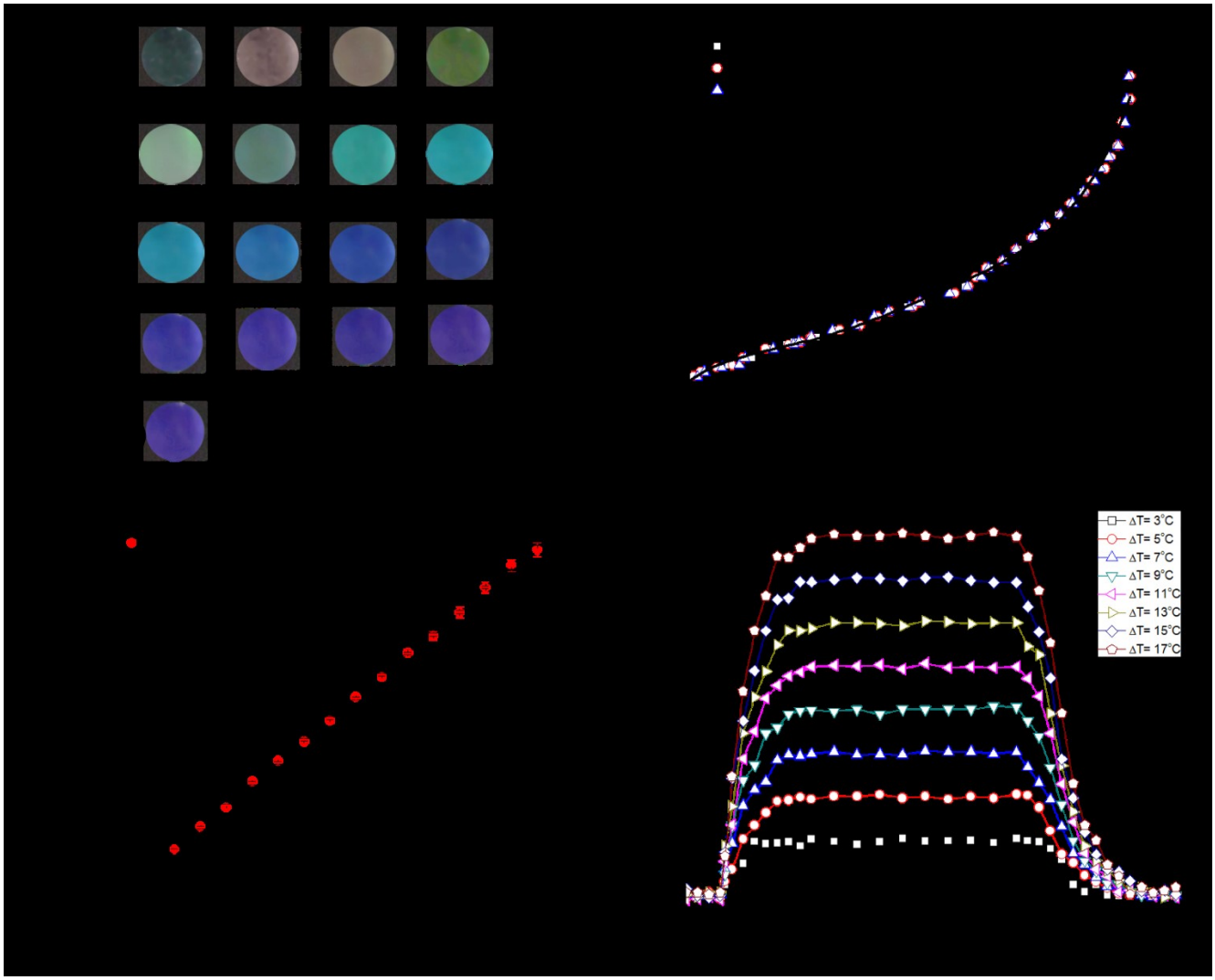

Figure 4.4: (a) Digital image of a temperature sensing unit at different temperatures with gaussian filter. (b) Hue-Temperature calibration of el-TLC composite material; black line here is the fitted polynomial curve. (c) Comparison of el-TLC and IR based temperature sensing. (d) The real time response of the temperature sensor with varying temperature difference between active surface and ambience.

$$\delta T = \left[\left(\frac{dT}{dh}\delta h\right)^2 + (2 * SE)^2\right]^{1/2} \qquad 4.2$$

where, ${}^{dT}/_{dh}$ is the slope of fitting polynomial curve. SE is the standard error of estimation and can be computed by following equation (181):

$$SE = \left[\sum_{n=1}^{m} (T_n(h) - T_{fit,n}(h)) / (m - n - 1)\right]^{1/2} \quad 4.3$$

The calculated SE value for our calibration curve was 0.03. The temperature values extracted from this hue-temperature relation of el-TLC composite was compared with the values from IR camera (Seek Thermal). We found that in temperature range of 26ºC to 36ºC, our el-TLC system could predict the temperature with uncertainty of 0.1ºC or lower (Figure 4.4(d)), which is of the same sensitivity as IR camera. Above 36ºC, due of higher hue values, δT starts to increase sharply and reaches to 0.2ºC at T= 40ºC, which is still quite reasonable sensitivity value for such an inexpensive temperature sensing platform with TLC material.

The temperature response of a TLC material is typically in the range of milliseconds (180). So, the response time of our temperature sensor will only be dependent on the rate of heat transfer through el-CB and hydrogel layers. The heating and cooling response time was measured by placing the individual sensing unit on a Peltier stage set at constant temperature, and then let it cool down in ambient condition (T= 23ºC) while continuously monitoring the surface temperature using IR camera. The response time varies with the temperature difference between the testing surface and ambient (Figure 4.4 (d)), as ΔT will determine the heat transfer between the layers. The response time, here, was defined as the duration it takes for the surface to reach 90% of the temperature set for the Peltier stage. So, for example, in case of ΔT= 17ºC, the response time was 26 seconds while for ΔT= 7ºC, it was 28 seconds.

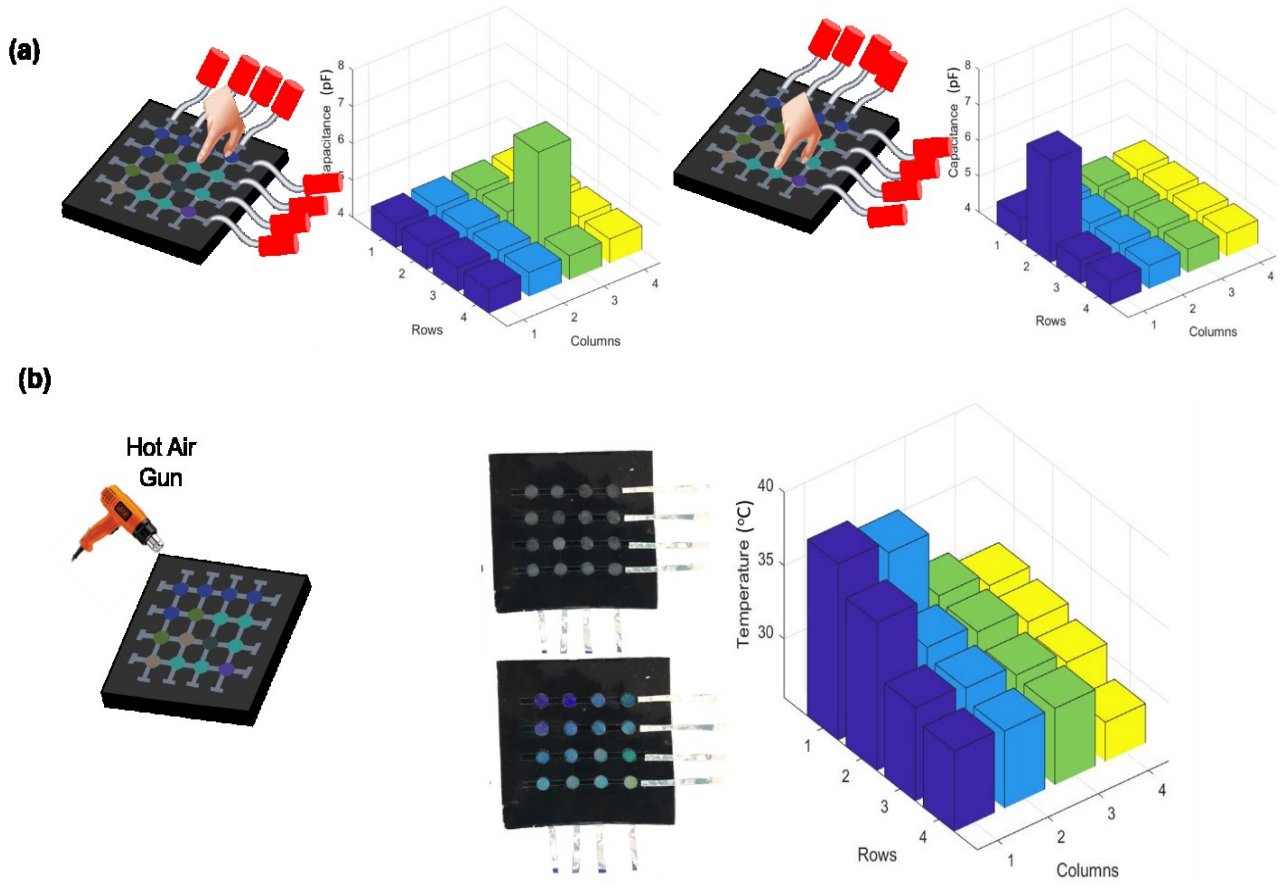

Figure 4.5: (a) Tactile and (b) temperature sensing of our 4x4 array pressure-temperature bimodal sensor

Finally, we examined the multi-pixel operation of our 4 × 4 bifunctional sensors array with 16 independent pressure and temperature detecting pixels. For each pixel, initial capacitance was measured to be 4.65 ±0.04 pF. When a pixel was pressed with a finger, that sensing unit had an increase in capacitance (6.80 ±0.12 pF) while the others remained at their original values (Figure 4.5(a)), thus locating the touch is possible. All the multiplexed capacitance data acquisition was carried out by channel-by-channel measurements through LCR meter (There is an immediate plan to switch to electronic circuit board for simultaneous data acquisition of all 16 pixels). To observe temperature sensing from different pixels, we blow a hot air gun from top-left side of the device. In response to the increase in temperature, the color of the sensing units changed. Figure 4.5(b)

derived from a snapshot at a certain time after blowing the hot air. Here, Gaussian filter was applied to all pixel locations to remove noise coming from dust particles and to compensate for non-uniform illumination of PDMS-TLC pixels. Then, we extracted the temperature values from each pixel by using the hue-temperature relation. The units which were present near the hot air gun had higher hue values, which corresponds to higher temperature. The opposite can be said for units falling far from the hot-air gun.

4.3 Conclusion

In summary, here we have demonstrated a bimodal e-skin device which is able to quantify both pressure and temperature through electrical and optical approaches respectively. The device comprises of a functioning layer of PDMS-TLC composite which performs dual function of dielectric layer for tactile sensing and photonic element for temperature measurement. The increase in dielectric permittivity of this composite layer improves the pressure sensitivity of the device. The chromatic interpretation of the TLC composite is calibrated by plotting a curve of hue vs temperature. With this relation, the temperature of a surface can be accurately measured with a digital image within an uncertainty values of less than 0.1 ^{o}C for temperatures ranging between 26 °C and 36 °C, and less than 0.2 ^{o}C between 36 °C and 42 °C. The use of elastomer and tough hydrogel patterns render this device mechanically robust, stretchable and deformable. With dual parameter sensing, easy fabrication steps and reasonable sensitivity, this device will have potential application in skin-like wearable and stretchable electronics

4.4 Experimental Section

4.4.1 Fabrication of el-TLC Composite & Working Layer

A known wt% of TLC slurry was added to the base of PDMS and thoroughly mixed together using mechanical stirring (Caframo's Digital- BDC 2002). Curing agent was then added into this mixture and the system was degassed in a vacuum chamber for 20 minutes to remove air bubbles. The base to curing agent ratio was maintained at 10:1.

To prepare the working layer we first adhered PET (polyethylene terephthalate) sheet onto a glass plate. PDMS layer of 100 μm was casted on this PET sheet using a spin coater. Using the CO_2 laser cutter small circles of diameter of 2 mm were etched in the PDMS layer at defined positions, determined by the location of sensing units in original device design. The trenches in trimmed PDMS layer were used as a template and el-TLC pre-polymer was instilled into them using a syringe. Excess amount was removed carefully using a sharp scalpel. The whole setup was placed in an oven at 80ºC to fully cure the el-TLC pixels.

4.4.2 Fabrication of el-CB Templates

A small amount of carbon black (Sigma Aldrich) was added to the base of 1:1 mixture of toluene and PDMS. The mixture was magnetically stirred for 1 hour at 60 ºC. It is important to note that carbon black to PDMS ratio was kept to 50:1 which was insignificant to have any effect on the conductivity of PDMS. After proper mixing toluene was allowed to evaporate by placing the mixture at 120ºC after which curing agent of was thoroughly mixed with it. This el-CB pre-polymer was casted using a 300 μm PMMA mold mounted on a glass slide. Before casting, the prepolymer was degassed for 20 minutes to remove air bubbles created during the mixing process. The el-CB casts were then cut into definite patterns using a CO_2 laser cutter to get the templates.

4.4.3 Fabrication of PAm Hydrogel Patterns

We followed the protocol by Li *et al*. (112) to prepare PAm hydrogels. Briefly, Sodium 4-vinylbenzenesulfonate (NaSS; anionic comonomer) and [3-(methacryloylamino) propyl] trimethylammonium chloride (MPTC; cationic comonomer) were added and mixed together in 1 M NaCl solution; the concentration of both charged comonomers in the final solution was 1M. The amount of photoinitiator (Irgacure 2959) added was 0.1 mole% of the total monomers. This solution was then purged with nitrogen gas for 15 minutes and then injected in between two transparent PET sheets separated by a 400 μm silicone spacer. The whole set up was sandwiched between two glass-slides and then placed in a UV chamber (Wavelength = 365 nm (free from 185 nm light); Intensity = 22mW/cm^2) to carry out the random free radical polymerization for 8 hours. After polymerization reaction, the glass slides were removed while PET sheets were stay put during laser cutting to prevent hydrogels to dry out from focused beam. PET layers were eventually removed only prior to placing the hydrogel patterns into el-CB templates.

4.4.4 Fabrication of e-skin Device

All the key fabrication steps involved, for device construction, are schematically represented in Figure 4.2(c). At first, working layer was sandwiched between the two perpendicularly placed el-CB templates using PDMS-Toluene mortar. To prepare PDMS-toluene mortar as adhesive layer, we borrowed the procedure from Chueh *et al*. (177). At first, PMDS was mixed with toluene in 1:1 weight ratio using a vortex mixer. This diluted PDMS solution was then spin coated on a glass plate using a spin coater (3 sec; 500 rpm). The el-CB templates were brought in contact of this spin-coated layer of PDMS-toluene mortar, and let it stay there for 30 seconds. This process ensured that only contact surfaces of el-CB templates were selectively coated. The coated templates were then placed on top of the working layer or over-coatings (el-CB & PDMS) and

pressed gently by sandwiching between two glass slides. In the end the whole arrangement was placed on top of a hot plate, set at 50^{o}C, for 3 hours to fully cure the adhesive layer of PDMS. The patterns in el-CB templates were filled with ionically conductive PAm hydrogels patterns and they were electrically connected with aluminium tapes. Next, we cast 50 μm layers of PDMS and el-CB on top of PET sheets using a spin coater. PDMS-Toluene mortar was then applied to these layers and device was sandwiched between them using glass slides and alligator clips. The setup was placed on a hotplate, set at 50^{o}C. After 3 hours of curing, the PET sheets could easily be removed, and hydrogel patterns were sealed.

Chapter 5. Conclusion

This work attempts to explore the potential of tough polyampholyte (PAm) hydrogels in the field of energy storage devices and stretchable electronics.

We started with Chapter 1 where we provided the current status of tough hydrogels in the fields of stretchable electronics and energy storage devices. In Chapter 2, we explained the physics behind the fracture-mechanics of hyperelastic materials (hydrogels and elastomers). This was followed by a thorough elaboration of various strategies and concepts that have been undertaken, over the years, to prepare hydrogels which are mechanically tough.

In Chapter 3 we advocated the practice of using tough PAm hydrogels as gel electrolyte for energy applications for number of reasons- (1) They have high water retention ability and show anti-polyelectrolyte effect: this allows them to uptake more electrolyte which leads to higher ionic conductivity. (2) PAm hydrogels bear charged ionic groups and strong diploes on their surface that makes them self-healable and imparts them with the ability to form an intimate contact with the electrodes- an essential requirement for energy storage devices. (3) According to our observations, when tough PAm hydrogels are dialyzed in different electrolyte solutions, they deliver high ionic conductivity while still maintaining good mechanical properties- a condition that is rarely observed in gel electrolytes.

In Chapter 4, we used tough PAm hydrogels, in their as-prepared state, as transparent and stretchable electrodes for a thermochromic liquid crystal (TLC) based bi-functional e-skin device that can detect pressure and temperature stimuli, simultaneously, without any cross-interference between sensors. Our e-skin device had a multi-layered structure with a functional layer of PDMS-

TLC composite acting both as dielectric layer for capacitive sensing of pressure and photonic element to measure temperature fluctuations through digital image processing. It was required to have a transparent conductive material as electrode for capacitive pressure sensors so that they do not obstruct any optical signal coming form PDMS-TLC layer. Ionically conductive, transparent PAm hydrogels were an ideal choice of material to perform this task. Also, the self-adhesive nature of PAm hydrogels helped in binding all the layers together and thus, provided the structural integrity to our device.

Over the years, huge amount of efforts has been made to introduce toughening mechanisms in hydrogels that render them mechanically tough. However, only in recent times their application in some of the unconventional fields, with unprecedent scope, have been realized. This thesis work is a step forward in exploiting the unique properties of tough hydrogels, specifically polyampholyte hydrogels, to realize their true potential from an end-user perspective. However, there are some opportunities where the scope of this thesis can be extended. For example, in our bi-functional sensing device we had to, manually, carry out digital image processing of each pixel for temperature measurements. A separate algorithm or software can be developed which can automatically locate the sensing pixels in the device and perform image processing in one go. Further, a micro-structured pattern of PDMS-TLC composite can also be used to further improve the tactile sensing of the device at low pressure.

References

1. Omidian H, Park K. Introduction to hydrogels. In Biomedical applications of hydrogels handbook. New York: Springer; 2010. p. 1-16.

2. Hoare TR, Kohane DS. Hydrogels in drug delivery: Progress and challenges. Polymer. 2008 Apr 15; 49(8): p. 1993-2007.

3. Tavakoli J, Tang Y. Hydrogel Based Sensors for Biomedical Applications: An Updated Review. Polymers. 2017 Aug 16; 9(8): p. 364.

4. De Gennes PG, Okumura K, Shahinpoor M, Kim KJ. Mechanoelectric effects in ionic gels. EPL (Europhysics Letters). 2000 May 15; 50(4): p. 513.

5. Lee KY, Mooney DJ. Hydrogels for tissue engineering. Chemical reviews. 2001 Jul 11; 101(7): p. 1869-80.

6. Malkoch M, Vestberg R, Gupta N, Mespouille L, Dubois P, Mason AF, Hedrick JL, Liao Q, Frank CW, Kingsbury K, Hawker CJ. Synthesis of well-defined hydrogel networks using click chemistry. Chemical Communications. 2006; 26: p. 2774-6.

7. Sakai T, Matsunaga T, Yamamoto Y, Ito C, Yoshida R, Suzuki S, Sasaki N, Shibayama M, Chung UI. Design and fabrication of a high-strength hydrogel with ideally homogeneous network structure from tetrahedron-like macromonomers. Macromolecules. 2008 Jun 21; 41(14): p. 5379-84.

8. Haque MA, Kurokawa T, Gong JP. Super tough double network hydrogels and their application as biomaterials. Polymer. 2012 Apr 17; 53(9): p. 1805-22.

9. Sun JY, Zhao X, Illeperuma WR, Chaudhuri O, Oh KH, Mooney DJ, Vlassak JJ, Suo Z. Highly stretchable and tough hydrogels. Nature. 2012 Sep 6; 489(7414): p. 133-6.

10. Gong JP. Why are double network hydrogels so tough? Soft Matter. 2010; 6(12): p. 2583-90.

11. Yang CH, Chen B, Zhou J, Chen YM, Suo Z. Electroluminescence of giant stretchability. Advanced Materials. 2016 Jun 1; 28(22): p. 4480-4.

12. La TG, Li X, Kumar A, Fu Y, Yang S, Chung HJ. Highly Flexible, Multipixelated Thermosensitive Smart Windows Made of Tough Hydrogels. ACS applied materials & interfaces. 2017 Sep 13; 9(38): p. 33100-6.

13. Yuk H, Lin S, Ma C, Takaffoli M, Fang NX, Zhao X. Hydraulic hydrogel actuators and robots optically and sonically camouflaged in water. Nature communications. 2017 Feb 1; 8: p. 14230.

14. Guo J, Liu X, Jiang N, Yetisen AK, Yuk H, Yang C, Khademhosseini A, Zhao X, Yun SH. Highly stretchable, strain sensing hydrogel optical fibers. Advanced Materials. 2016 Dec 1; 28(46): p. 10244-9.

15. Lin S, Yuk H, Zhang T, Parada GA, Koo H, Yu C, Zhao X. Stretchable hydrogel electronics and devices. Advanced Materials. 2016 Jun 1; 28(22): p. 4497-505.

16. Yu C, Duan Z, Yuan P, Li Y, Su Y, Zhang X, Pan Y, Dai LL, Nuzzo RG, Huang Y, Jiang H. Electronically Programmable, Reversible Shape Change in Two-and Three-Dimensional Hydrogel Structures. Advanced Materials. 2013 Mar 20; 25(11): p. 1541-6.

17. Keplinger C, Sun JY, Foo CC, Rothemund P, Whitesides GM, Suo Z. Stretchable, transparent, ionic conductors. Science. 2013 Aug 30; 341(6149): p. 984-7.

18. Kim CC, Lee HH, Oh KH, Sun JY. Highly stretchable, transparent ionic touch panel. Science. 2016 Aug 12; 353(6300): p. 682-7.

19. Sun JY, Keplinger C, Whitesides GM, Suo Z. Ionic skin. Advanced Materials. 2014 Dec 1; 26(45): p. 7608-14.

20. Larson C, Peele B, Li S, Robinson S, Totaro M, Beccai L, Mazzolai B, Shepherd R. Highly stretchable electroluminescent skin for optical signaling and tactile sensing. Science. 2016 Mar 4; 351(6277): p. 1071-4.

21. Yang P, Mai W. Flexible solid-state electrochemical supercapacitors. Nano Energy. 2014 Sep 1; 8: p. 274-90.

22. Meng C, Liu C, Chen L, Hu C, Fan S. Highly flexible and all-solid-state paperlike polymer supercapacitors. Nano letters. 2010 Sep 10; 10(10): p. 4025-31.

23. Yang CC, Hsu ST, Chien WC. All solid-state electric double-layer capacitors based on alkaline polyvinyl alcohol polymer electrolytes. Journal of power sources. 2005 Dec 1; 152: p. 303-10.

24. Wang G, Lu X, Ling Y, Zhai T, Wang H, Tong Y, Li Y. LiCl/PVA gel electrolyte stabilizes vanadium oxide nanowire electrodes for pseudocapacitors. ACS nano. 2012 Oct 16; 6(11): p. 10296-302.

25. Zhong C, Deng Y, Hu W, Qiao J, Zhang L, Zhang J. A review of electrolyte materials and compositions for electrochemical supercapacitors. Chemical Society Reviews. 2015; 44(21): p. 7484-539.

26. Hallinan Jr DT, Balsara NP. Polymer electrolytes. Polymer electrolytes. Annual review of materials research. 2013 Jul 1; 43: p. 503-25.

27. Shi Y, Peng L, Yu G. Nanostructured conducting polymer hydrogels for energy storage applications. Nanoscale. 2015; 7(30): p. 12796-806.

28. Shi Y, Pan L, Liu B, Wang Y, Cui Y, Bao Z, Yu G. Nanostructured conductive polypyrrole hydrogels as high-performance, flexible supercapacitor electrodes. Journal of Materials Chemistry A. 2014; 2(17): p. 6086-91.

29. Pan L, Yu G, Zhai D, Lee HR, Zhao W, Liu N, Wang H, Tee BC, Shi Y, Cui Y, Bao Z. Hierarchical nanostructured conducting polymer hydrogel with high electrochemical activity. Proceedings of the National Academy of Sciences. 2012 Jun 12; 109(24): p. 9287-92.

30. Inglis CE. Stresses in a plate due to the presence of cracks and sharp corners. Spie Milestone series MS. 1997; 137: p. 3-17.

31. Bouchbinder E, Goldman T, Fineberg J. The dynamics of rapid fracture: instabilities, nonlinearities and length scales. Reports on Progress in Physics. 2014 Mar 19; 77(4): p. 046501.

32. Griffith AA. The phenomena of rupture and flow in solids. Philosophical transactions of the royal society of london. Series A, containing papers of a mathematical or physical character. 1921 Jan 1; 221: p. 163-98.

33. Irwin GR. Fracture dynamics. Fracturing of metals. 1948; 147: p. 166.

34. Freund LB. Dynamic fracture mechanics: Cambridge university press; 1998 Mar 28.

35. Rice JR. Mathematical analysis in the mechanics of fracture. In Fracture: an advanced treatise.; 1968. p. 191-311.

36. Rice JR. A path independent integral and the approximate analysis of strain concentration by notches and cracks. Journal of applied mechanics. 1968 Jun 1; 35(2): p. 379-86.

37. Hui CY, Ruina A, Long R, Jagota A. Cohesive zone models and fracture. The Journal of Adhesion. 2011 Jan 25; 87(1): p. 1-52.

38. Barenblatt GI. The mathematical theory of equilibrium cracks in brittle fracture. Advances in applied mechanics. 1962 Dec 31; 7: p. 55-129.

39. Calvert P. Hydrogels for soft machines. Advanced materials. 2009 Feb 16; 21(7): p. 743-56.

40. Anderson IA, Gisby TA, McKay TG, O'Brien BM, Calius EP. Multi-functional dielectric elastomer artificial muscles for soft and smart machines. Journal of Applied Physics. 2012 Aug 15; 112(4): p. 041101.

41. Lake GJ, Thomas AG. The strength of highly elastic materials. In Proceedings of the Royal Society of London A: Mathematical, Physical and Engineering Sciences; 1967 Aug 22: The Royal Society. p. 108-119.

42. Hong W, Liu Z, Suo Z. Inhomogeneous swelling of a gel in equilibrium with a solvent and mechanical load. International Journal of Solids and Structures. 2009 Aug 15; 46(17): p. 3282-9.

43. Wang X, Hong W. Delayed fracture in gels. Soft Matter. 2012; 8(31): p. 8171-8.

44. Zhao X. A theory for large deformation and damage of interpenetrating polymer networks. Journal of the Mechanics and Physics of Solids. 2012 Feb 29; 60(2): p. 319-32.

45. Hong W, Wang X. A phase-field model for systems with coupled large deformation and mass transport. Journal of the Mechanics and Physics of Solids. 2013 Jun 30; 61(6): p. 1281-94.

46. Zhao X. Multi-scale multi-mechanism design of tough hydrogels: building dissipation into stretchy networks. Soft Matter. 2014; 10(5): p. 672-87.

47. Rivlin RS, Thomas AG. Rupture of rubber. I. Characteristic energy for tearing. J. Polym. Sci. 1953; 10: p. 291–318.

48. Baumberger T, Caroli C, Martina D. Solvent control of crack dynamics in a reversible hydrogel. Nature materials. 2006 Jul 1; 5(7): p. 552-5.

49. Shibayama M. Feature Article Spatial inhomogeneity and dynamic fluctuations of polymer gels. Macromol. Chem. Phys. 1998 Jan; 199(1): p. 1-30.

50. Panyukov S, Rabin Y. Polymer gels: frozen inhomogeneities and density fluctuations. Macromolecules. 1996 Nov 18; 29(24): p. 7960-75.

51. Candau S, Bastide J, Delsanti M. Structural, elastic, and dynamic properties of swollen polymer networks. In Polymer Networks.: Springer Berlin Heidelberg; 1982. p. 27-71.

52. Furukawa H, Horie K, Nozaki R, Okada M. Swelling-induced modulation of static and dynamic fluctuations in polyacrylamide gels observed by scanning microscopic light scattering. Physical Review E. 2003 Sep 22; 68(3): p. 031406.

53. Naficy S, Brown HR, Razal JM, Spinks GM, Whitten PG. Progress toward robust polymer hydrogels. Australian Journal of Chemistry. 2011 Sep 9; 64(8): p. 1007-25.

54. Mark JE, Erman B. Rubberlike elasticity: a molecular primer: Cambridge University Press; 2007 Feb 8.

55. Norisuye T, Masui N, Kida Y, Ikuta D, Kokufuta E, Ito S, Panyukov S, Shibayama M. Small angle neutron scattering studies on structural inhomogeneities in polymer gels: irradiation cross-linked gels vs chemically cross-linked gels. Polymer. 2002 Sep 1; 43(19): p. 5289-97.

56. Wang X, Wang H, Brown HR. Jellyfish gel and its hybrid hydrogels with high mechanical strength. Soft Matter. 2011; 7(1): p. 211-9.

57. Xu XD, Chen CS, Wang ZC, Wang GR, Cheng SX, Zhang XZ, Zhuo RX. “Click” chemistry for in situ formation of thermoresponsive P (NIPAAm-co-HEMA)-based hydrogels. Journal of Polymer Science Part A: Polymer Chemistry. 2008 Aug 1; 46(15): p. 5263-77.

58. van Dijk M, van Nostrum CF, Hennink WE, Rijkers DT, Liskamp RM. Synthesis and characterization of enzymatically biodegradable PEG and peptide-based hydrogels prepared by click chemistry. Biomacromolecules. 2010 May 24; 11(6): p. 1608-14.

59. Crescenzi V, Cornelio L, Di Meo C, Nardecchia S, Lamanna R. Novel hydrogels via click chemistry: synthesis and potential biomedical applications. Biomacromolecules. 2007 Jun 11; 8(6): p. 1844-50.

60. Ossipov DA, Hilborn J. Poly (vinyl alcohol)-based hydrogels formed by “click chemistry”. Macromolecules. 2006 Mar 7; 39(5): p. 1709-18.

61. Matsunaga T, Sakai T, Akagi Y, Chung UI, Shibayama M. Structure characterization of tetra-PEG gel by small-angle neutron scattering. Macromolecules. 2009 Feb 3; 42(4): p. 1344-51.

62. Okumura Y, Ito K. The polyrotaxane gel: A topological gel by figure-of-eight cross-links. Advanced Materials. 2001 Apr 1; 13(7): p. 485-7.

63. Karino T, Okumura Y, Zhao C, Kataoka T, Ito K, Shibayama M. SANS studies on deformation mechanism of slide-ring gel. Macromolecules. 2005 Jul 12; 38(14): p. 6161-7.

64. Gong JP, Katsuyama Y, Kurokawa T, Osada Y. Double-network hydrogels with extremely high mechanical strength. Advanced Materials. 2003 Jul 17; 15(14): p. 1155-8.

65. Nakajima T, Sato H, Zhao Y, Kawahara S, Kurokawa T, Sugahara K, Gong JP. A universal molecular stent method to toughen any hydrogels based on double network concept. Advanced Functional Materials. 2012 Nov 7; 22(21): p. 4426-32.

66. Chen Q, Zhu L, Zhao C, Wang Q, Zheng J. A Robust, One-Pot Synthesis of Highly Mechanical and Recoverable Double Network Hydrogels Using Thermoreversible Sol-Gel Polysaccharide. Advanced Materials. 2013 Aug 14; 25(30): p. 4171-6.

67. Na YH, Tanaka Y, Kawauchi Y, Furukawa H, Sumiyoshi T, Gong JP, Osada Y. Necking phenomenon of double-network gels. Macromolecules. 2006 Jul 11; 39(14): p. 4641-5.

68. De Gennes PG. Soft adhesives. Langmuir. 1996 Sep 18; 12(19): p. 4497-500.

69. Brown HR. A model of the fracture of double network gels. Macromolecules. 2007 May 15; 40(10): p. 3815-8.

70. Okumura K. Toughness of double elastic networks. EPL (Europhysics Letters). 2004 Aug; 67(3): p. 470.

71. Tanaka Y. A local damage model for anomalous high toughness of double-network gels. EPL (Europhysics Letters). 2007 May 22; 78(5): p. 56005.

72. Tanaka Y, Kawauchi Y, Kurokawa T, Furukawa H, Okajima T, Gong JP. Localized Yielding Around Crack Tips of Double-Network Gels. Macromolecular Rapid Communications. 2008 Sep 17; 29(18): p. 1514-20.

73. Yu QM, Tanaka Y, Furukawa H, Kurokawa T, Gong JP. Direct observation of damage zone around crack tips in double-network gels. Macromolecules. 2009 Jun 23; 42(12): p. 3852-5.

74. Chen Q, Chen H, Zhu L, Zheng J. Fundamentals of double network hydrogels. Journal of Materials Chemistry B. 2015; 3(18): p. 3654-76.

75. Nakajima T, Furukawa H, Tanaka Y, Kurokawa T, Gong JP. Effect of void structure on the toughness of double network hydrogels. Journal of Polymer Science Part B: Polymer Physics. 2011 Sep 1; 49(17): p. 1246-54.

76. Nakajima T, Fukuda Y, Kurokawa T, Sakai T, Chung UI, Gong JP. Synthesis and fracture process analysis of double network hydrogels with a well-defined first network. ACS Macro Letters. 2013 May 30; 2(6): p. 518-21.

77. Sun TL, Kurokawa T, Kuroda S, Ihsan AB, Akasaki T, Sato K, Haque MA, Nakajima T, Gong JP. Physical hydrogels composed of polyampholytes demonstrate high toughness and viscoelasticity. Nature materials. 2013 Oct 1; 12(10): p. 932-7.

78. Ihsan AB, Sun TL, Kuroda S, Haque MA, Kurokawa T, Nakajima T, Gong JP. A phase diagram of neutral polyampholyte–from solution to tough hydrogel. Journal of Materials Chemistry B. 2013; 1(36): p. 4555-62.

79. Ihsan AB, Sun TL, Kurokawa T, Karobi SN, Nakajima T, Nonoyama T, Roy CK, Luo F, Gong JP. Self-healing behaviors of tough polyampholyte hydrogels. Macromolecules. 2016 May 23; 49(11): p. 4245-52.

80. Agrawal A, Rahbar N, Calvert PD. Strong fiber-reinforced hydrogel. Acta biomaterialia. 2013 Feb 28; 9(2): p. 5313-8.

81. Jang J, Oh H, Lee J, Song TH, Jeong YH, Cho DW. A cell-laden nanofiber/hydrogel composite structure with tough-soft mechanical property. Applied Physics Letters. 2013 May 27; 102(21): p. 211914.

82. Moutos FT, Freed LE, Guilak F. A biomimetic three-dimensional woven composite scaffold for functional tissue engineering of cartilage. Nature materials. 2007 Feb 1; 6(2): p. 162-7.

83. Haraguchi K, Takehisa T. Nanocomposite hydrogels: a unique organic-inorganic network structure with extraordinary mechanical, optical, and swelling/de-swelling properties. Advanced Materials. 2002 Aug 16; 14(16): p. 1120.

84. Haraguchi K, Juan-Jun L. Mechanical Properties of Nano-composite Hydrogels Consisting of Organic/Inorganic Networks and the Effects of Clay Modification thereto. JOURNAL OF NETWORK POLYMER JAPAN. 2004; 25(1): p. 2-12.

85. Haraguchi K. Synthesis and properties of soft nanocomposite materials with novel organic/inorganic network structures. Polymer journal. 2011 Mar 1; 43(3): p. 223-41.

86. Haraguchi K, Li HJ, Matsuda K, Takehisa T, Elliott E. Mechanism of forming organic/inorganic network structures during in-situ free-radical polymerization in PNIPA-clay nanocomposite hydrogels. Macromolecules. 2005 Apr 19; 38(8): p. 3482-90.

87. Abdurrahmanoglu S, Okay O. Rheological behavior of polymer–clay nanocomposite hydrogels: Effect of nanoscale interactions. Journal of applied polymer science. 2010 May 15; 116(4): p. 2328-35.

88. Nishida T, Endo H, Osaka N, Li HJ, Haraguchi K, Shibayama M. Deformation mechanism of nanocomposite gels studied by contrast variation small-angle neutron scattering. Physical Review E. 2009 Sep 14; 80(3): p. 030801.

89. Lin WC, Fan W, Marcellan A, Hourdet D, Creton C. Large strain and fracture properties of poly (dimethylacrylamide)/silica hybrid hydrogels. Macromolecules. 2010 Feb 4; 43(5): p. 2554-63.

90. Gaharwar AK, Rivera CP, Wu CJ, Schmidt G. Transparent, elastomeric and tough hydrogels from poly (ethylene glycol) and silicate nanoparticles. Acta biomaterialia. 2011 Dec 31; 7(12): p. 4139-48.

91. Gaharwar AK, Dammu SA, Canter JM, Wu CJ, Schmidt G. Highly extensible, tough, and elastomeric nanocomposite hydrogels from poly (ethylene glycol) and hydroxyapatite nanoparticles. Biomacromolecules. 2011 Mar 17; 12(5): p. 1641-50.

92. Liu J, Chen C, He C, Zhao J, Yang X, Wang H. Synthesis of graphene peroxide and its application in fabricating super extensible and highly resilient nanocomposite hydrogels. Acs Nano. 2012 Aug 28; 6(9): p. 8194-202.

93. Lin WC, Marcellan A, Hourdet D, Creton C. Effect of polymer–particle interaction on the fracture toughness of silica filled hydrogels. Soft Matter. 2011; 7(14): p. 6578-82.

94. Wang Q, Hou R, Cheng Y, Fu J. Super-tough double-network hydrogels reinforced by covalently compositing with silica-nanoparticles. Soft Matter. 2012; 8(22): p. 6048-56.

95. Huang T, Xu HG, Jiao KX, Zhu LP, Brown HR, Wang HL. A novel hydrogel with high mechanical strength: a macromolecular microsphere composite hydrogel. Advanced Materials. 2007 Jun 18; 19(12): p. 1622-6.

96. Xu K, Tan Y, Chen Q, An H, Li W, Dong L, Wang P. A novel multi-responsive polyampholyte composite hydrogel with excellent mechanical strength and rapid shrinking rate. Journal of colloid and interface science. 2010 May 15; 345(2): p. 360-8.

97. Meid J, Dierkes F, Cui J, Messing R, Crosby AJ, Schmidt A. Richtering W. Mechanical properties of temperature sensitive microgel/polyacrylamide composite hydrogels—from soft to hard fillers. Soft Matter. 2012; 8(15): p. 4254-63.

98. Hu J, Kurokawa T, Hiwatashi K, Nakajima T, Wu ZL, Liang SM, Gong JP. Structure optimization and mechanical model for microgel-reinforced hydrogels with high strength and toughness. Macromolecules. 2012 Jun 5; 45(12): p. 5218-28.

99. Karuppasamy K, Kim HS, Kim D, Vikraman D, Prasanna K, Kathalingam A, Sharma R, Rhee HW. An enhanced electrochemical and cycling properties of novel boronic Ionic liquid based ternary gel polymer electrolytes for rechargeable Li/LiCoO 2 cells. Scientific Reports. 2017 Sep 11; 7(1): p. 11103.

100. Yu H, Wu J, Fan L, Xu K, Zhong X, Lin Y, Lin J. Improvement of the performance for quasi-solid-state supercapacitor by using PVA–KOH–KI polymer gel electrolyte. Electrochimica Acta. 2011 Aug 1; 56(20): p. 6881-6.

101. Choudhury NA, Sampath S, Shukla AK. Hydrogel-polymer electrolytes for electrochemical capacitors: an overview. Energy & Environmental Science. 2009; 2(1): p. 55-67.

102. Chodankar NR, Dubal DP, Lokhande AC, Lokhande CD. Ionically conducting PVA–LiClO4 gel electrolyte for high performance flexible solid state supercapacitors. Journal of colloid and interface science. 2015 Dec 15; 460: p. 370-6.

103. Qu QT, Wang B, Yang LC, Shi Y, Tian S, Wu YP. Study on electrochemical performance of activated carbon in aqueous Li2SO4, Na2SO4 and K2SO4 electrolytes. Electrochemistry Communications. 2008 Oct 1; 10(10): p. 1652-5.

104. Chae JH, Chen GZ. Influences of ions and temperature on performance of carbon nano-particulates in supercapacitors with neutral aqueous electrolytes. Particuology. 2014 Aug 1; 15: p. 9-17.

105. Shin WK, Cho J, Kannan AG, Lee YS, Kim DW. Cross-linked composite gel polymer electrolyte using mesoporous methacrylate-functionalized SiO 2 nanoparticles for lithium-ion polymer batteries. Scientific reports. 2016 May 18; 6: p. 26332.

106. Wang Y, Zhong WH, Schiff T, Eyler A, Li B. A Particle-Controlled, High-Performance, Gum-Like Electrolyte for Safe and Flexible Energy Storage Devices. Advanced Energy Materials. 2015 Jan 1; 5(2).

107. Bhattacharya A, Ray P. Studies on surface tension of poly (vinyl alcohol): effect of concentration, temperature, and addition of chaotropic agents. Journal of applied polymer science. 2004 Jul 5; 93(1): p. 122-30.

108. Peng X, Liu H, Yin Q, Wu J, Chen P, Zhang G, Liu G, Wu C, Xie Y. A zwitterionic gel electrolyte for efficient solid-state supercapacitors. Nature communications. 2016 May 26; 7: p. 11782.

109. Lee CJ, Wu H, Hu Y, Young M, Wang H, Lynch D, Xu F, Cong H, Cheng G. Ionic Conductivity of Polyelectrolyte Hydrogels. ACS Applied Materials & Interfaces. 2018; 10(6): p. 5845-5852.

110. Wang F, Yang J, Zhao J. Understanding anti-polyelectrolyte behavior of a well-defined polyzwitterion at the single-chain level. Polymer International. 2015 Aug 1; 64(8): p. 999-1005.

111. Li X, Liu L, Wang X, Ok YS, Elliott JA, Chang SX, Chung HJ. Flexible and Self-Healing Aqueous Supercapacitors for Low Temperature Applications: Polyampholyte Gel Electrolytes with Biochar Electrodes. Scientific reports. 2017 May 10; 7(1): p. 1685.

112. Li X, Charaya H, Bernard GM, Elliott JA, Michaelis, Lee B, VK, Chung HJ. Low-Temperature Ionic Conductivity Enhanced by Disrupted Ice Formation in Polyampholyte Hydrogels. Macromolecules. .

113. Jiang M, Zhu J, Chen C, Lu Y, Ge Y, Zhang X. Poly (vinyl Alcohol) Borate Gel Polymer Electrolytes Prepared by Electrodeposition and Their Application in Electrochemical Supercapacitors. ACS applied materials & interfaces. 2016 Jan 29; 8(5): p. 3473-81.

114. Wang Z, Tao F, Pan Q. A self-healable polyvinyl alcohol-based hydrogel electrolyte for smart electrochemical capacitors. Journal of Materials Chemistry A. 2016; 4(45): p. 17732-9.

115. Jiang X, Xiang N, Zhang H, Sun Y, Lin Z, Hou L. Preparation and characterization of poly (vinyl alcohol)/sodium alginate hydrogel with high toughness and electric conductivity. Carbohydrate polymers. 2018 Apr 15; 186: p. 377-83.

116. Zhao C, Wang C, Yue Z, Shu K, Wallace GG. Intrinsically stretchable supercapacitors composed of polypyrrole electrodes and highly stretchable gel electrolyte. ACS applied materials & interfaces. 2013 Sep 5; 5(18): p. 9008-14.

117. Zangi R. Can salting-in/salting-out ions be classified as chaotropes/kosmotropes? The Journal of Physical Chemistry B. 2009 Dec 8; 114(1): p. 643-50.

118. Chen X, Flores SC, Lim SM, Zhang Y, Yang T, Kherb J, Cremer PS. Specific anion effects on water structure adjacent to protein monolayers. Langmuir. 2010 Jun 18; 26(21): p. 16447-54.

119. Zhang Y, Furyk S, Bergbreiter DE, Cremer PS. Specific ion effects on the water solubility of macromolecules: PNIPAM and the Hofmeister series. Journal of the American Chemical Society. 2005 Oct 19; 127(41): p. 14505-10.

120. Dyakonova MA, Berezkin AV, Kyriakos K, Gkermpoura S, Popescu MT, Filippov SK, Štěpánek P, Di Z, Tsitsilianis C, Papadakis CM. Salt-Induced Changes in Triblock Polyampholyte Hydrogels: Computer Simulations and Rheological, Structural, and Dynamic Characterization. Macromolecules. 2015 Nov 4; 48(22): p. 8177-89.

121. Jaspers M, Rowan AE, Kouwer PH. uning hydrogel mechanics using the hofmeister effect. Advanced Functional Materials. 2015 Nov 1; 25(41): p. 6503-10.

122. Zhang Z, Moxey M, Alswieleh A, Morse AJ, Lewis AL, Geoghegan M, Leggett GJ. Effect of salt on phosphorylcholine-based zwitterionic polymer brushes. Langmuir. 2016 May 10; 32(20): p. 5048-57.

123. Xiao S, Zhang Y, Shen M, Chen F, Fan P, Zhong M, Ren B, Yang J, Zheng J. Structural Dependence of Salt-Responsive Polyzwitterionic Brushes with Anti-polyelectrolyte Effect. Langmuir. 2017 Dec.

124. Yang J, Chen H, Xiao S, Shen M, Chen F, Fan P, Zhong M, Zheng J. Salt-responsive zwitterionic polymer brushes with tunable friction and antifouling properties. Langmuir. 2015 Aug 13; 31(33): p. 9125-33.

125. Wang T, Wang X, Long Y, Liu G, Zhang G. Ion-specific conformational behavior of polyzwitterionic brushes: exploiting it for protein adsorption/desorption control. Langmuir. 2013 May 22; 29(22): p. 6588-96.

126. Kohonen MM, Karaman ME, Pashley RM. Debye Length in Multivalent Electrolyte Solution. Langmuir. 2000 Jun 27; 16(13): p. 5749-53.

127. Collins KD. Charge density-dependent strength of hydration and biological structure. Biophysical journal. 1997 Jan 1; 72(1): p. 65-76.

128. He Y, Shao Q, Chen S, Jiang S. Chaotrope vs. kosmotrope: Which one has lower friction? The Journal of chemical physics. 2011 Oct 21; 135(15): p. 154702.

129. Pegram LM, Record Jr MT. Thermodynamic origin of Hofmeister ion effects. The journal of physical chemistry B. 2008 Jul 16; 112(31): p. 9428-36.

130. Seckbach J, Oren A, Stan-Lotter H. Polyextremophiles: life under multiple forms of stress: Springer Science & Business Media; 2013 May 13.

131. Xu L, Li X, Zhai M, Huang L, Peng J, Li J, Wei G. Ion-specific swelling of poly (styrene sulfonic acid) hydrogel. The Journal of Physical Chemistry B. 2007 Apr 5; 111(13): p. 3391-7.

132. Tripathi BP, Shahi VK. 3-[[3-(Triethoxysilyl) propyl] amino] propane-1-sulfonic acid− poly (vinyl alcohol) cross-linked zwitterionic polymer electrolyte membranes for direct methanol fuel cell applications. ACS applied materials & interfaces. 2009 Apr 28; 1(5): p. 1002-12.

133. Li H, Erbaş A, Zwanikken J, Olvera de la Cruz M. Ionic conductivity in polyelectrolyte hydrogels. Macromolecules. 2016 Nov 16; 49(23): p. 9239-46.

134. Saito Y, Okano M, Kubota K, Sakai T, Fujioka J, Kawakami T. Evaluation of interactive effects on the ionic conduction properties of polymer gel electrolytes. The Journal of Physical Chemistry B. 2012 Aug 10; 116(33): p. 10089-97.

135. Cardoso J, Huanosta A, Manero O. Ionic conductivity studies on salt-polyzwitterion systems. Macromolecules. 1991 May; 24(10): p. 2890-5.

136. Dahiya RS, Valle M. Robotic tactile sensing: technologies and system: Springer Science & Business Media; 2012.

137. Zhao S, Zhu R. Electronic skin with multifunction sensors based on thermosensation. Advanced Materials. 2017 Apr 1; 29(15).

138. Someya, T., Sekitani, T., Iba, S., Kato, Y., Kawaguchi, H. and Sakurai, T. A large-area, flexible pressure sensor matrix with organic field-effect transistors for artificial skin applications. Proceedings of the National Academy of Sciences of the United States of America. 2004 Jul 6; 101(27): p. 9966-70.

139. Persano L, Dagdeviren C, Su Y, Zhang Y, Girardo S, Pisignano D, Huang Y, Rogers JA. High performance piezoelectric devices based on aligned arrays of nanofibers of poly (vinylidenefluoride-co-trifluoroethylene). Nature communications. 2013 Mar 27; 4: p. 1633.

140. Ramuz M, Tee BC, Tok JB, Bao Z. Transparent, optical, pressure-sensitive artificial skin for large-area stretchable electronics. Advanced Materials. 2012 Jun 26; 24(24): p. 3223-7.

141. Tee BC, Wang C, Allen R, Bao Z. An electrically and mechanically self-healing composite with pressure-and flexion-sensitive properties for electronic skin applications. Nature nanotechnology. 2012 Dec; 7(12): p. 825.

142. Wang X, Gu Y, Xiong Z, Cui Z, Zhang T. Silk-molded flexible, ultrasensitive, and highly stable electronic skin for monitoring human physiological signals. Advanced materials. 2014 Mar 1; 26(9): p. 1336-42.

143. Kim SY, Park S, Park HW, Park DH, Jeong Y, Kim DH. Highly sensitive and multimodal all-carbon skin sensors capable of simultaneously detecting tactile and biological stimuli. Advanced Materials. 2015 Jul 1; 27(28): p. 4178-85.

144. Zhang F, Zang Y, Huang D, Di CA, Zhu D. Flexible and self-powered temperature–pressure dual-parameter sensors using microstructure-frame-supported organic thermoelectric materials. Nature communications. 2015 Sep 21; 6: p. 8356.

145. Park J, Kim M, Lee Y, Lee HS, Ko H. Fingertip skin–inspired microstructured ferroelectric skins discriminate static/dynamic pressure and temperature stimuli. Science advances. 2015 Oct 1; 1(9): p. e1500661.

146. Pang C, Lee GY, Kim TI, Kim SM, Kim HN, Ahn SH, Suh KY. A flexible and highly sensitive strain-gauge sensor using reversible interlocking of nanofibres. Nature materials. 2012 Sep; 11(9): p. 795.

147. Sekitani T, Someya T. Stretchable, large-area organic electronics. Advanced Materials. 2010 May 25; 22(20): p. 2228-46.

148. Zirkl M, Sawatdee A, Helbig U, Krause M, Scheipl G, Kraker E, Ersman PA, Nilsson D, Platt D, Bodö P, Bauer S. An All-Printed Ferroelectric Active Matrix Sensor Network Based on Only Five

Functional Materials Forming a Touchless Control Interface. Advanced Materials. 2011 May 10; 23(18): p. 2069-74.

149. Wu W, Wen X, Wang ZL. Taxel-addressable matrix of vertical-nanowire piezotronic transistors for active/adaptive tactile imaging. Science. 2013 Apr 25;: p. 1234855.

150. Bae GY, Pak SW, Kim D, Lee G, Kim DH, Chung Y, Cho K. Linearly and Highly Pressure-Sensitive Electronic Skin Based on a Bioinspired Hierarchical Structural Array. Advanced Materials. 2016 Jul 1; 28(26): p. 5300-6.

151. Pang C, Koo JH, Nguyen A, Caves JM, Kim MG, Chortos A, Kim K, Wang PJ, Tok JB, Bao Z. Highly skin-conformal microhairy sensor for pulse signal amplification. Advanced materials. 2015 Jan 1; 27(4): p. 634-40.

152. Yang T, Wang W, Zhang H, Li X, Shi J, He Y, Zheng QS, Li Z, Zhu H. Tactile sensing system based on arrays of graphene woven microfabrics: electromechanical behavior and electronic skin application. ACS nano. 2015 Oct 16; 9(11): p. 10867-75.

153. Li X, Yang T, Yang Y, Zhu J, Li L, Alam FE, Li X, Wang K, Cheng H, Lin CT, Fang Y. Large-Area Ultrathin Graphene Films by Single-Step Marangoni Self-Assembly for Highly Sensitive Strain Sensing Application. Advanced Functional Materials. 2016 Mar 1; 26(9): p. 1322-9.

154. Hong SY, Lee YH, Park H, Jin SW, Jeong YR, Yun J, You I, Zi G, Ha JS. Stretchable active matrix temperature sensor array of polyaniline nanofibers for electronic skin. Advanced Materials. 2016 Feb 1; 28(5): p. 930-5.

155. Yokota T, Inoue Y, Terakawa Y, Reeder J, Kaltenbrunner M, Ware T, Yang K, Mabuchi K, Murakawa T, Sekino M, Voit W. Ultraflexible, large-area, physiological temperature sensors for multipoint measurements. Proceedings of the National Academy of Sciences. 2015 Nov 24; 112(47): p. 14533-8.

156. Ren X, Pei K, Peng B, Zhang Z, Wang Z, Wang X, Chan PK. A Low-Operating-Power and Flexible Active-Matrix Organic-Transistor Temperature-Sensor Array. Advanced Materials. 2016 Jun 1; 28(24): p. 4832-8.

157. Trung TQ, Ramasundaram S, Hwang BU, Lee NE. An All-Elastomeric Transparent and Stretchable Temperature Sensor for Body-Attachable Wearable Electronics. Advanced Materials. 2016 Jan 1; 28(3): p. 502-9.

158. Kim J, Lee M, Shim HJ, Ghaffari R, Cho HR, Son D, Jung YH, Soh M, Choi C, Jung S, Chu K. Stretchable silicon nanoribbon electronics for skin prosthesis. Nature Communications. 2014 Dec 9; 5: p. 5747.

159. Engel J, Chen J, Fan Z, Liu C. Polymer micromachined multimodal tactile sensors. Sensors and Actuators A: physical. 2005 Jan 3; 117(1): p. 50-61.

160. Kanao K, Harada S, Yamamoto Y, Honda W, Arie T, Akita S, Takei K. Highly selective flexible tactile strain and temperature sensors against substrate bending for an artificial skin. RSC Advances. 2015; 5(38): p. 30170-4.

161. Yeo WH, Kim YS, Lee J, Ameen A, Shi L, Li M, Wang S, Ma R, Jin SH, Kang Z, Huang Y. Multifunctional epidermal electronics printed directly onto the skin. Advanced Materials. 2013 May 28; 25(20): p. 2773-8.

162. Hua Q, Sun J, Liu H, Bao R, Yu R, Zhai J, Pan C, Wang ZL. Skin-inspired highly stretchable and conformable matrix networks for multifunctional sensing. Nature communications. 2018 Jan 16; 9(1): p. 244.

163. Zhao S, Zhu R. Flexible Bimodal Sensor for Simultaneous and Independent Perceiving of Pressure and Temperature Stimuli. Advanced Materials Technologies. 2017 Nov 1; 2(11).

164. Graz I, Krause M, Bauer-Gogonea S, Bauer S, Lacour SP, Ploss B, Zirkl M, Stadlober B, Wagner S. Flexible active-matrix cells with selectively poled bifunctional polymer-ceramic nanocomposite for pressure and temperature sensing skin. Journal of Applied Physics. 2009 Aug 1; 106(3): p. 034503.

165. Gerratt AP, Michaud HO, Lacour SP. Elastomeric electronic skin for prosthetic tactile sensation. Advanced Functional Materials. 2015 Apr 1; 25(15): p. 2287-95.

166. Choong CL, Shim MB, Lee BS, Jeon S, Ko DS, Kang TH, Bae J, Lee SH, Byun KE, Im J, Jeong YJ. Highly stretchable resistive pressure sensors using a conductive elastomeric composite on a micropyramid array. Advanced materials. 2014 Jun 1; 26(21): p. 3451-8.

167. Khan ZU, Edberg J, Hamedi MM, Gabrielsson R, Granberg H, Wågberg L, Engquist I, Berggren M, Crispin X. Thermoelectric polymers and their elastic aerogels. Advanced Materials. 2016 Jun 1; 28(22): p. 4556-62.

168. Yu C, Li Y, Zhang X, Huang X, Malyarchuk V, Wang S, Shi Y, Gao L, Su Y, Zhang Y, Xu H. Adaptive optoelectronic camouflage systems with designs inspired by cephalopod skins. Proceedings of the National Academy of Sciences. 2014 Sep 9; 111(36): p. 12998-3003.

169. Park SI, Ahn JH, Feng X, Wang S, Huang Y, Rogers JA. Theoretical and experimental studies of bending of inorganic electronic materials on plastic substrates. Advanced Functional Materials. 2008 Sep 23; 18(18): p. 2673-84.

170. Hsu YS, Wang L, Liu WF, Chiang YJ. Temperature compensation of optical fiber Bragg grating pressure sensor. IEEE Photonics Technology Letters. 2006 Apr 1; 18(7): p. 874-6.

171. Hammock ML, Chortos A, Tee BC, Tok JB, Bao Z. 25th anniversary article: the evolution of electronic skin (e-skin): a brief history, design considerations, and recent progress. Advanced materials. 2013 Nov; 25(42): p. 5997-6038.

172. Gao L, Zhang Y, Malyarchuk V, Jia L, Jang KI, Webb RC, Fu H, Shi Y, Zhou G, Shi L, Shah D. Epidermal photonic devices for quantitative imaging of temperature and thermal transport characteristics of the skin. Nature communications. 2014 Sep 19; 5: p. 4938.

173. Kim G, Cho S, Chang K, Kim WS, Kang H, Ryu SP, Myoung J, Park J, Park C, Shim W. Spatially Pressure-Mapped Thermochromic Interactive Sensor. Advanced Materials. 2017 Apr 1; 29(13).

174. Yu C, Zhang Y, Cheng D, Li X, Huang Y, Rogers JA. All-elastomeric, strain-responsive thermochromic color indicators. Small. 2014 Apr 1; 10(7): p. 1266-71.

175. Ashforth-Frost S. Quantitative thermal imaging using liquid crystals. Journal of biomedical optics. 1996 Jan; 1(1): p. 18-28.

176. Li Q, Zhang LN, Tao XM, Ding X. Review of flexible temperature sensing networks for wearable physiological monitoring. Advanced healthcare materials. 2017 Jun 21.

177. Chueh BH, Huh D, Kyrtsos CR, Houssin T, Futai N, Takayama S. Leakage-free bonding of porous membranes into layered microfluidic array systems. Analytical chemistry. 2007 May 1; 79(9): p. 3504-8.

178. Chou HH, Nguyen A, Chortos A, To JW, Lu C, Mei J, Kurosawa T, Bae WG, Tok JB, Bao Z. A chameleon-inspired stretchable electronic skin with interactive colour changing controlled by tactile sensing. Nature communications. 2015 Aug 24; 6: p. 8011.

179. Farina DJ, Hacker JM, Moffat RJ, Eaton JK. Illuminant invariant calibration of thermochromic liquid crystals. Experimental thermal and fluid Science. 1994 Jul 1; 9(1): p. 1-2.

180. Stasiek J, Stasiek A, Jewartowski M, Collins MW. Liquid crystal thermography and true-colour digital image processing. Optics & Laser Technology. 2006 Jun 1; 38(4-6): p. 243-56.

181. Hay JL, Hollingsworth DK. Calibration of micro-encapsulated liquid crystals using hue angle and a dimensionless temperature. Experimental thermal and fluid science. 1998 Nov 1; 18(3): p. 251-7.